Advances and Physicochemical Property Investigations by Methylene Chain Length of Perovskite-type Layer Crystals [NH3(CH2)nNH3]CdCl4 (n=2, 3, and 4)

Ae Ran Lim (aeranlim@hanmail.net)
Jeonju University

Research Article

Keywords: Hybrid perovskites, potential applications, several electrochemical devices, organic–inorganic perovskite

Posted Date: May 28th, 2021

DOI: https://doi.org/10.21203/rs.3.rs-530081/v1

ARTICLE

Advances and physicochemical property investigations by methylene chain length of perovskite-type layer crystals $[NH_3(CH_2)_nNH_3]CdCl_4$ (n=2, 3, and 4)

Ae Ran Lim

Hybrid perovskites have potential applications in several electrochemical devices such as supercapacitors, batteries, and fuel cells. However, despite various potential applications, there have been limited studies on compounds containing Cd. Therefore, in this study, the structures and phase transition temperatures T_C of organic–inorganic perovskite $[NH_3(CH_2)_nNH_3]CdCl_4$ (n=2, 3, and 4) were confirmed by X-ray diffraction and DSC experiments. The thermal stabilities obtained by TGA and DTA results were considered as a function of the length n of the CH_2 groups in the cation. In addition, structural characteristics and molecular dynamics of the cation and anion near T_C were studied by ^{1}H MAS NMR, ^{13}C MAS NMR, ^{14}N static NMR, and ^{113}Cd MAS NMR experiments. From these results, regardless of whether n is even or odd, the differences in thermal and physical properties were minimal. Rather, the difference in molecular motion relative to the length of the cation was seen only at higher temperatures. These results provide insights into the thermal stability and molecular dynamics of $[NH_3(CH_2)_nNH_3]CdCl_4$ crystals and are expected to facilitate potential applications.

The organic–inorganic hybrid perovskite crystals $[NH_3(CH_2)_nNH_3]MX_4$ (n=2, 3, 4,…; M=Mn, Fe, Co, Cu, Zn, Cd,…; X=Cl and Br) have drawn significant research interest. Their physicochemical properties depend on factors such as the characteristics of the organic cations and geometry of the inorganic metal halide anions constituting the crystal.[1-10] The organic cation of the hybrid complex contributes to properties such as structural flexibility and optical properties, whereas the inorganic anion is responsible for the thermal and mechanical properties. In the case of M=Mn, Cu, and Cd, the crystal structures consist of alternate octahedron $(MX_6)^{2-}$ and organic chains. In the case of M=Co and Zn, isolated tetrahedral structures are formed, where an inorganic layer of $(MX_4)^{2-}$ is sandwiched between the layers of an organic cation.[11-15] Furthermore, several studies focusing on their molecular structure have reported an even-odd effect as the number of carbon atoms in the diammonium chain changes, which affects the structural properties of these materials.[16] Structural phase transitions have also been reported for $[NH_3(CH_2)_nNH_3]MX_4$ types, in which the link between adjacent octahedral or tetrahedral planes is realized by methylene chains bearing NH_3 groups on both ends. The $[NH_3(CH_2)_nNH_3]$ organic chains extend along the longest c-axis. Perovskite, $[NH_3(CH_2)_nNH_3]CdCl_4$ (M=Cd, X=Cl), consists of puckered layers of $CdCl_6$ separated by nearly perpendicular layers of $[NH_3(CH_2)_nNH_3]$ chains. The distance between the two neighboring inorganic layers depends on the length of the organic chain.[17] These compounds have attracted considerable interest owing to the multiplicity of their crystal structures, which govern their thermodynamic properties and structural

Department of Carbon Convergence Engineering, Jeonju University, Jeonju 55069, Korea. [2]Department of Science Education, Jeonju University, Jeonju 55069, Korea. email: arlim@jj.ac.kr

dynamics. These hybrid perovskites have potential applications in several electrochemical devices such as supercapacitors, batteries, and fuel cells.[18-23]

The synthesis and characterization of $[NH_3(CH_2)_2NH_3]CdCl_4$ with n=2 were first discussed by Batcaglia et al.[24] Subsequently, the X-ray results for this crystal structure at 298 K were reported by Lamhamdi et al.[25] The phase transition at 375 K for the $[NH_3(CH_2)_3NH_3]CdCl_4$ crystal with n=3 is reversible and continuous, according to previous dielectric and optical studies.[26, 27] In addition, the structural, thermal, and vibrational properties as well as molecular motions have been characterized by Staskiewicz et al.[6] Recently, the physicochemical properties of this crystal were reported by our group.[28] In the case of n=4, the thermodynamic and crystallographic characters of the phase transitions for $NH_3(CH_2)_4NH_3CdCl_4$ were studied, and the crystal structure in each phase was discussed from X-ray diffraction measurements.[16, 29] However, despite various potential applications, there have been limited studies on compounds containing Cd. In particular, the thermal properties, structural phase transitions, and structural dynamics resulting from differences in the methylene chain length of $[NH_3(CH_2)_nNH_3]CdCl_4$ crystals have not been discussed in detail.

This study aims to investigate the thermodynamic properties and molecular dynamics of $[NH_3(CH_2)_nNH_3]CdCl_4$ as a function of the length n of CH_2 groups in the carbon chain. The crystal structures, phase transition temperatures, and thermodynamic properties of the crystals with n=2, 3, and 4 are investigated using X-ray diffraction, differential scanning calorimetry (DSC), thermogravimetric analysis (TGA), and differential thermal analysis (DTA). In addition, the chemical shifts and spin-lattice relaxation time $T_{1\rho}$ are probed using ^{1}H magic angle spinning nuclear magnetic resonance (MAS NMR), ^{13}C MAS NMR, and static ^{14}N NMR as a function of temperature to elucidate the characteristics of the $[NH_3(CH_2)_nNH_3]$ cation. Furthermore, the chemical shifts for ^{113}Cd MAS NMR are recorded as a function of the temperature in order to understand the geometry of octahedral $CdCl_6$. The results provide insights into the thermodynamic properties and structural dynamics of $[NH_3(CH_2)_nNH_3]CdCl_4$ crystals based on the length and even–odd effect of the organic chain and are expected to facilitate potential applications in the future.

Crystal structures

1,2-Ethylenediammonium tetrachlorocadmate, $[NH_3(CH_2)_2NH_3]CdCl_4$ (n=2), crystallizes in the monoclinic form with space group $P2_1/a$, and this crystal does not exhibit any structural phase transitions. The unit cell parameters are a=7.292 Å, b=7.344 Å, c=8.609 Å, β=92.74°, and Z=2.[25] $[NH_3(CH_2)_2NH_3]$ cations are situated between the layers and are linked to the layers via an N–H···Cl hydrogen-bonding network. The Cd atom is located on an inversion center, and the coordination environment is described as a highly distorted octahedral.[24] 1,3-Propylenediammonium tetrachlorocadmate, $[NH_3(CH_2)_3NH_3]CdCl_4$ (n=3), is known to undergo a structural phase transition at T_C = 375 K.[6, 24] At room temperature, the crystals are orthorhombic with the space group *Pman*. The unit cell has the following parameters: a=7.373 Å, b=7.523

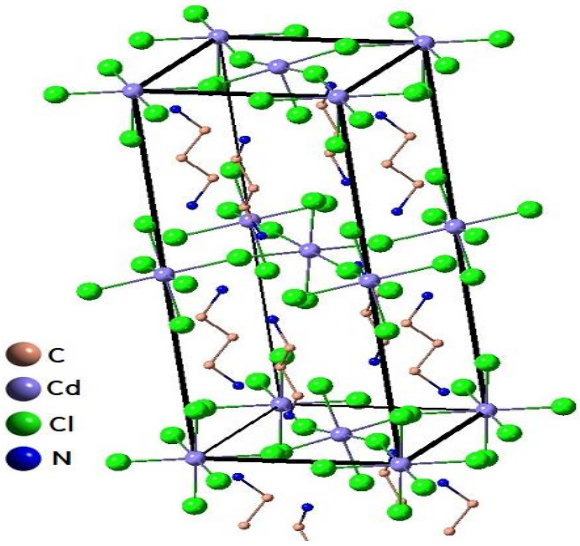

Figure 1. The structure of $[NH_3(CH_2)_3NH_3]CdCl_4$ crystal at room temperature.

Å, *c*=19.111 Å, and *Z*=4. When the temperature is above T_C, the crystal is still orthorhombic; however, the space group becomes *Imma*, and the lattice constants become *a*=7.38577 Å, *b*=7.56974 Å, *c*=18.7300 Å, and *Z*=4.[6] Figure 1 shows the structure of the $[NH_3(CH_2)_3NH_3]CdCl_4$ crystal at 300 K. In each formula unit, the six hydrogen atoms in ammonium form hydrogen bonds N–H···Cl. The Cd atom is surrounded by six Cl atoms to form nearly regular $CdCl_6$ octahedra. 1,4-Butanediyldiammonium tetrachlorocadmate, $[NH_3(CH_2)_4NH_3]CdCl_4$ (*n*=4), undergoes two structural phase transitions near 338 K (=T_{C2}) and 367 K (=T_{C1}).[16] The phases III and II are monoclinic, whereas the high temperature phase I is orthorhombic. At phases III and II, it is monoclinic, with space group $P2_1/a$ and Z = 2. The unit cell parameters in phase III are *a*=7.657 Å, *b*=7.585 Å, *c*=9.541 Å, and *β*=101.56°.[16] Further, the lattice parameters in phase II are *a*=7.48 Å, *b*=7.53 Å, *c*=10.18 Å, and *β*=97.5°. The high-temperature phase I is orthorhombic, with space group *Pman* and Z=2. The unit cell parameters are *a*=7.377 Å, *b*=7.538 Å, and *c*=10.600 Å. Structural information for the three compounds are summarized in Table 1.

Table 1. The structures, phase transition temperatures (T_C), lattice constants, and Cd-Cl distances of $[NH_3(CH_2)_nNH_3]CdCl_4$ (*n*=2, 3, and 4) crystals.

	Structure	T_C (K)	Lattice constants (Å)	Cd-Cl (average Å)
n=2	Monoclinic	x	*a*=7.292, *b*=7.344, *c*=8.609, *β*=92.74°	2.616
n=3	Orthorhombic	375 (T_C)	*a*=7.373, *b*=7.523, *c*=19.111 ($T < T_C$)	2.6288
	Orthorhombic		*a*=7.38577, *b*=7.56974, *c*=18.7300 ($T > T_C$)	2.6073
n=4	Monoclinic	338 (T_{C2}) 367 (T_{C1})	*a*=7.657, *b*=7.585, *c*=9.541, *β*=101.56° ($T < T_{C2}$)	2.646
	Monoclinic		*a*=7.48, *b*=7.53, *c*=10.18, *β*=97.5° ($T_{C2} < T < T_{C1}$)	
	Orthorhombic		*a*=7.377, b=7.538, c=10.600 ($T > T_{C1}$)	2.6198

Experimental

An aqueous solution containing $NH_2(CH_2)_nNH_2{\cdot}2HCl$ and $CdCl_2$ was slowly evaporated at 300 K to produce single crystals of $[NH_3(CH_2)_nNH_3]CdCl_4$ (*n*=2, 3, and 4). The structures of the $[NH_3(CH_2)_nNH_3]CdCl_4$ crystals at 298 K were analyzed using an X-ray diffraction system equipped with a Cu-Kα radiation source.[30] The lattice parameters were determined by single-crystal X-ray diffraction at the Seoul Western Center of the Korea Basic Science Institute (KBSI). The crystals were mounted on a Bruker D8 Venture equipped with an 1 μS micro-focus sealed tube Mo-Kα and a PHOTON III M14 detector.[30]

DSC (DSC 25, TA Instruments) measurements for the three crystals were carried out at a scanning speed of 10 °C/min between 190 and 600 K under nitrogen gas. TGA and DTA experiments were performed on a thermogravimetric analyzer (TA Instrument) at the same heating rate between 300 and 873 K under N_2 gas.[31] In addition, optical observations were made using an optical polarizing microscope in the temperature range of 300–680 K, where the as-grown single crystals were placed on the heating stage of a Linkam THM-600.

NMR spectra of $[NH_3(CH_2)_nNH_3]CdCl_4$ crystals were obtained using a Bruker 400 MHz Avance II+ solid-state NMR spectrometer equipped with 4 mm MAS probes at the Seoul Western Center, KBSI. The Larmor frequencies for ^1H MAS NMR and ^{13}C MAS NMR experiments were 400.13 and 100.61 MHz, respectively. The MAS rate to minimize the spinning sideband was 10 kHz, and the NMR chemical shifts were recorded using tetramethylsilane (TMS) as the standard.[32] The $T_{1\rho}$ values were obtained using a $\pi/2-\tau$ pulse followed by a spin-lock pulse of duration τ, and the width of the $\pi/2$ pulse for ^1H and ^{13}C was in the range

of 3.4–3.62 μs. In addition, static ^{14}N NMR and ^{113}Cd MAS NMR spectra were measured with Larmor frequencies of 28.90 and 88.75 MHz, respectively. The ^{14}N NMR experiments were performed using a solid-state echo sequence: 4 μs–τ–4 μs–τ; τ=5 μs for n=2, τ=8 μs for n=3 and 4. The ^{113}Cd MAS NMR experiments were performed using a π/2−τ pulse followed by a spin-lock pulse of duration τ, and the width of the π/2 pulse for ^{113}Cd was 3.2 μs. The chemical shift measurements referenced NH_4NO_3 and $CdCl_2O_8{\cdot}6H_2O$ as standard samples. The temperature was changed by adjusting the nitrogen gas flow and heater current, and it was maintained within ±0.5 K.

Experimental results

Crystal structures

The X-ray powder diffraction patterns of the $[NH_3(CH_2)_nNH_3]CdCl_4$ crystals (n=2, 3, and 4) at 298 K are shown in Fig. 2. The lattice constants for the $[NH_3(CH_2)_2NH_3]CdCl_4$ crystal with n=2 are determined to be a=7.297 ± 0.002 Å, b=7.336 ± 0.002 Å, c=8.623 ± 0.002 Å, and β=92.810 ± 0.011°, and those for $[NH_3(CH_2)_3NH_3]CdCl_4$ with n=3 are determined to be a=7.351 ± 0.006 Å, b=7.486 ± 0.005 Å, and c=19.031 ± 0.014 Å. In the case of $[NH_3(CH_2)_4NH_3]CdCl_4$ with n=4, the lattice parameters are determined to be a=7.663 ± 0.003 Å, b=7.593 ± 0.002 Å, c=9.514 ± 0.002 Å, and β=101.616 ± 0.016°. These results are consistent with those reported previously.[6, 16, 24-26]

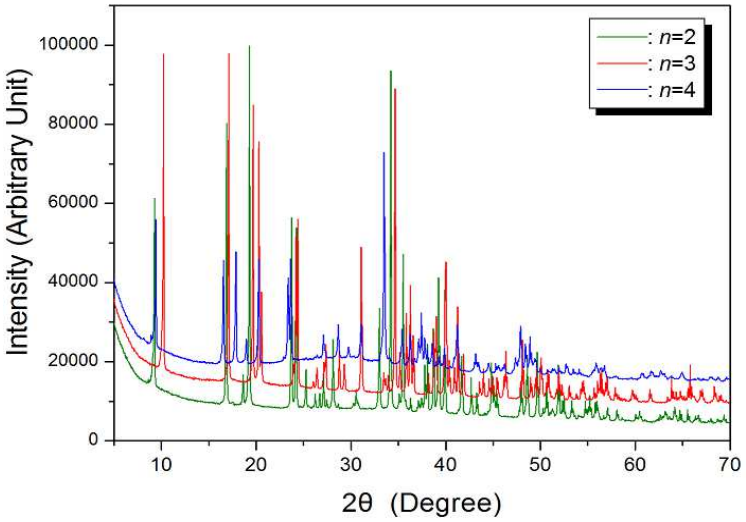

Figure 2. X-ray diffraction patterns of $[NH_3(CH_2)_nNH_3]CdCl_4$ (n=2, 3, and 4) at 298 K.

Phase transition temperatures and thermal properties

The DSC curves of $[NH_3(CH_2)_nNH_3]CdCl_4$ crystals at a heating rate of 10 K/min under a nitrogen atmosphere are shown in Fig. 3. No peak was observed for the case of n=2, whereas only one endothermic peak for

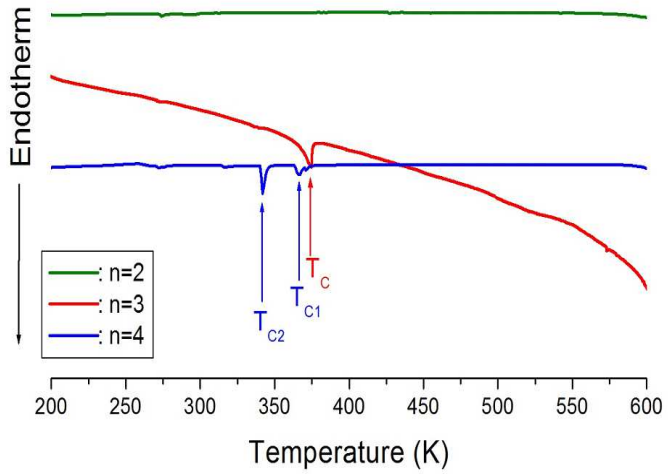

Figure 3. Differential scanning calorimetry (DSC) curves of $[NH_3(CH_2)_nNH_3]CdCl_4$ (n=2, 3, and 4).

n=3 was observed at 374 K (=T_C). Finally, for the case of n=4, two endothermic peaks were observed at 341 K (=T_{C2}) and 366 K (=T_{C1}). These phase transition temperatures are consistent with those reported previously.[6, 16, 27]

To verify whether the endothermic peaks correspond to phase transition or decomposition, TGA and DTA experiments were performed at the same heating rate. The TGA and DTA curves displayed in Fig. 4 show that the crystals with n = 2, 3, and 4 are almost stable up to approximately 493, 539, and 536 K, respectively; according to the number n of CH_2 groups in the carbon chain, the molecular weight loss near 493, 539, and 536 K marks the onset of partial thermal decomposition (at temperature T_d). $[NH_3(CH_2)_nNH_3]CdCl_4$ undergoes loss in the molecular weight with increasing temperature. The amount remaining as solid residues can be calculated from the molecular weights. When n=2, the loss of 12% and 23% of its weight at temperatures of about 622 K and 804 K was due to the decomposition of HCl and 2HCl, respectively (see Fig. 4(a)). The small endothermic peak at 374 K on the DTA curve for $[NH_3(CH_2)_3NH_3]CdCl_4$ is assigned to the phase transition detected in the DSC experiment. Additionally,

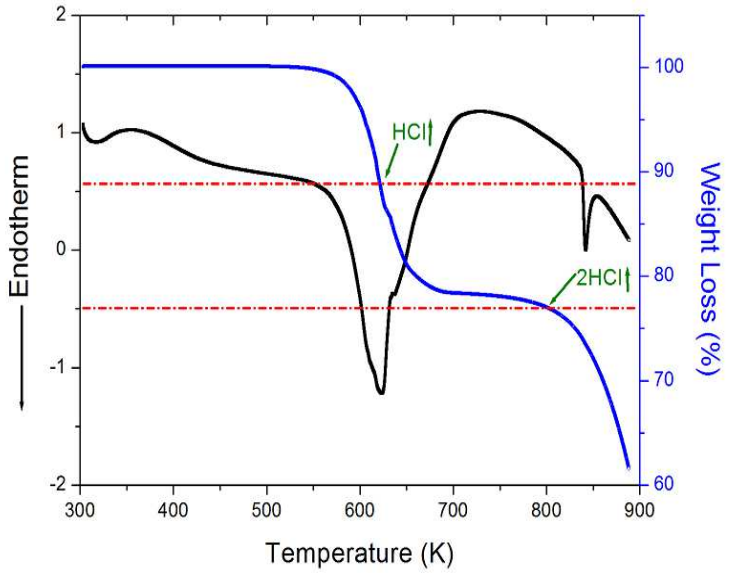

Figure 4(a). Thermogravimetric analysis (TGA) and differential thermal analysis (DTA) results of $[NH_3(CH_2)_2NH_3]CdCl_4$.

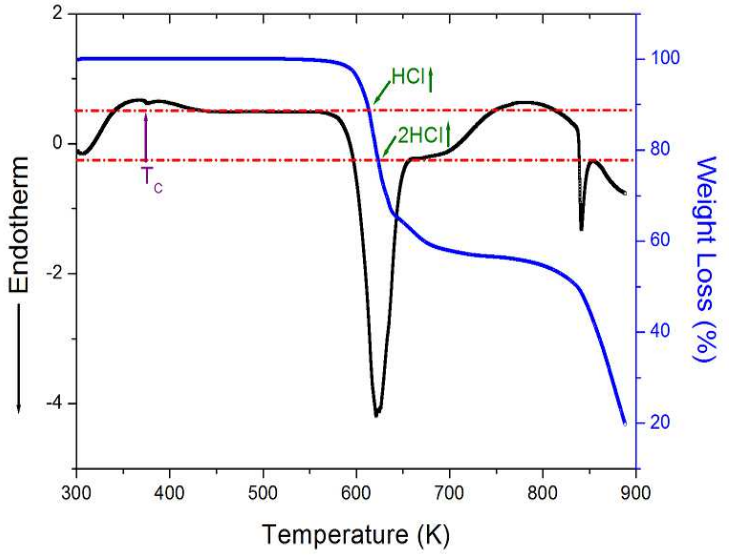

Figure 4(b). Thermogravimetric analysis (TGA) and differential thermal analysis (DTA) results of $[NH_3(CH_2)_3NH_3]CdCl_4$.

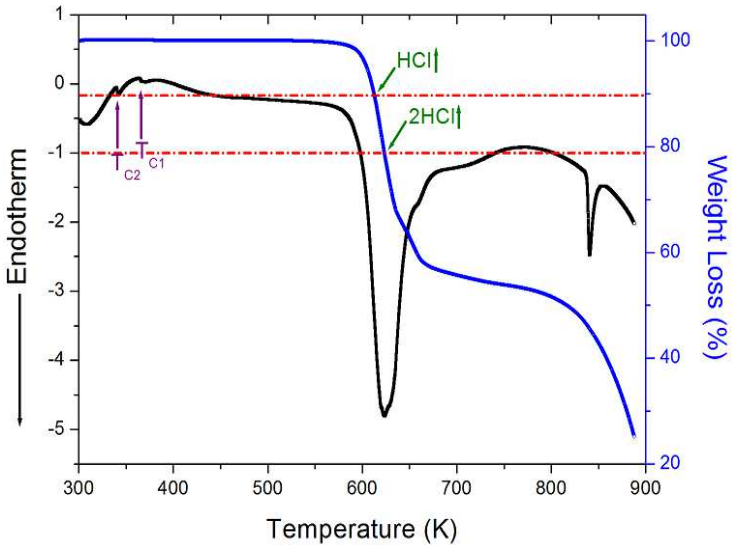

Figure 4(c). Thermogravimetric analysis (TGA) and differential thermal analysis (DTA) results of $[NH_3(CH_2)_4NH_3]CdCl_4$.

weight losses of 11% and 22% occurred at temperatures of 613 K and 623 K, respectively (see Fig. 4(b)). Finally, in the case of $[NH_3(CH_2)_4NH_3]CdCl_4$ crystals with *n*=4, the two small endothermic peaks at 341 K and 366 K on the DTA curve are attributed to the phase transition seen in the DSC result. At temperatures of 612 K and 623 K, 11% and 21% of its weight was respectively lost (see Fig. 4(c)). The molecular weight of the three crystals decreased sharply between 550 and 650 K. In the case of *n*=3 and 4 near 800 K, weight losses of 45% occurred, whereas when *n*=2, the weight loss was the smallest at 23%.

To support the TGA results, the appearance of single crystals with changing temperature was observed with an optical polarizing microscope (Fig. 5). For the case where *n*=2, the crystal formed at 300 K was colorless and transparent, while it appeared slightly opaque above 547 K. Upon increasing the temperature to 622 K, HCl was eliminated, and the crystal turned orange. Finally, the surface near 633 K appeared to melt slightly. For the case where *n*=3, the crystal had an opaque white color at room temperature. Upon increasing the temperature to 673 K, it remained opaque even though the 2HCl was blown away. For the case where *n*=4, the crystal was transparent at 300 K, and it turned opaque white with increasing temperature, likely indicating the elimination of HCl. Finally, it turned bright brown as 2HCl was lost near 670 K.

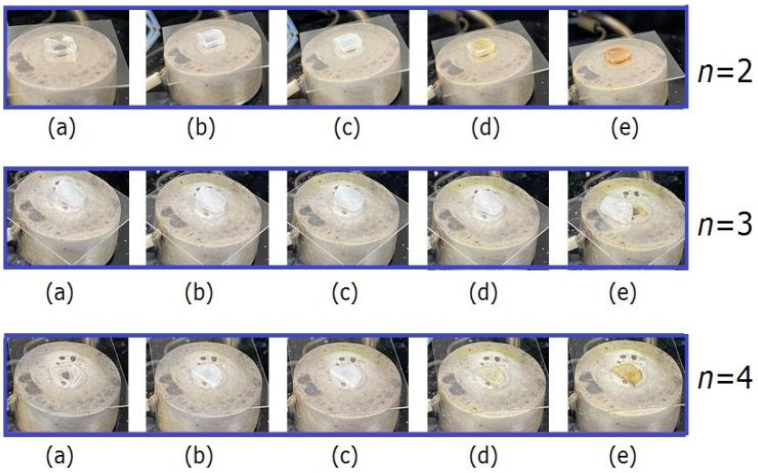

Figure 5. Changes in crystal by optical polarizing microscopy at (a) 300 K, (b) 547 K, (c) 573 K, (d) 622 K, and (e) 633 K for $[NH_3(CH_2)_2NH_3]CdCl_4$ with *n*=2; (a) 296 K, (b) 563 K, (c) 613 K, (d) 653 K, (e) 673 K for

$[NH_3(CH_2)_3NH_3]CdCl_4$ with *n*=3; and (a) 295 K, (b) 353 K, (c) 573 K, (d) 659 K, (e) 670 K for $[NH_3(CH_2)_4NH_3]CdCl_4$ with *n*=4.

^{1}H MAS NMR

The ^{1}H MAS NMR spectra of $[NH_3(CH_2)_nNH_3]CdCl_4$ crystals according to the length of the carbon chain were recorded as a function of temperature. The results of ^{1}H chemical shifts for *n*=2, 3, and 4 are shown in Fig. 6. At 300 K, the ^{1}H chemical shift for NH_3 and CH_2 were obtained at 7.96 and 4.78 ppm, respectively, in the case of *n*=2, and at 7.57 and 3.23 ppm, respectively, in the case of *n*=3. Finally, for *n*=4, they were obtained at 6.90 and 4.69 ppm, respectively. It can be seen that the ^{1}H chemical shifts for NH_3 when *n*=2, 3, and 4 are similar, while the ^{1}H chemical shifts for CH_2 are very different. In the case where *n*=3, no change was observed near T_C. In particular, in the case where *n*=4, the ^{1}H chemical shift for CH_2 shows discontinuity near T_{C2} and continuity near T_{C1}. The chemical shifts for NH_3 of all three crystals are nearly independent of temperature, which means that the surrounding environment of the ^{1}H in NH_3 does not significantly change with temperature. However, in the case where *n*=4, the surrounding environments of ^{1}H in CH_3 do significantly change with temperature.

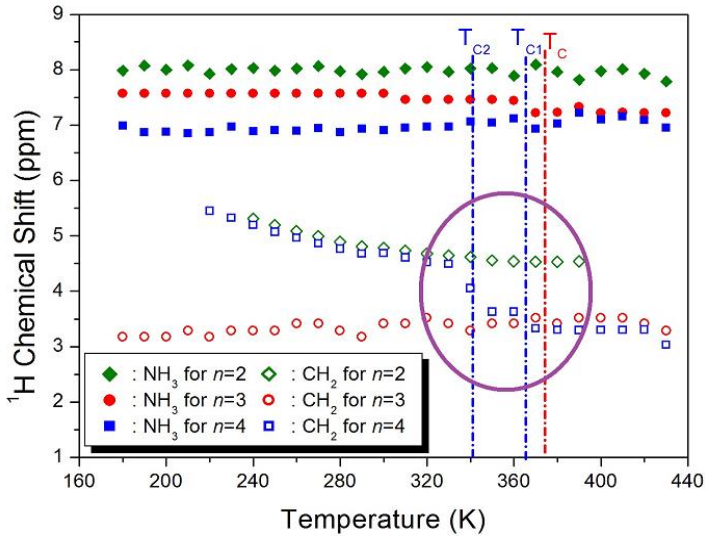

Figure 6. ^{1}H NMR chemical shifts for NH_3 and CH_2 in $[NH_3(CH_2)_nNH_3]CdCl_4$ (*n*=2, 3, and 4) as a function of temperature.

The ^{1}H MAS NMR spectra were measured with several delay times at each given temperature, and the plot of spectral intensities vs. delay times were found to follow a single exponential function. The decay rate of the spin-locked proton magnetization is characterized by the spin-lattice relaxation time $T_{1\rho}$ as[33-35]

$$P(\tau) = P(0)\exp(-\tau/T_{1\rho}), \quad (1)$$

where $P(\tau)$ and $P(0)$ are the signal intensities at time τ and τ=0, respectively. From the slope of the logarithm of intensities vs. delay times plot, the ^{1}H $T_{1\rho}$ values were determined for NH_3 and CH_2 at several temperatures. The ^{1}H $T_{1\rho}$ results are shown in Fig. 7 for the three compounds as a function of inverse temperature. In the cases where *n*=2 and 3, as the temperature increases, the $T_{1\rho}$ values increase rapidly from 1 to 700 *ms*, and then rapidly reduces at temperatures above 350 K. At 350 K, ^{1}H $T_{1\rho}$ has maximum values when *n*=2, and the values for NH_3 and CH_2 are 352 and 388 *ms*, respectively. The values when *n*=3 are 496 and 683 *ms*. In the case where *n*=2 and 3, as the temperature increases, the $T_{1\rho}$ values increase rapidly from 1 to 700 *ms*, and then rapidly reduces at temperatures above 350 K. At 350 K, ^{1}H $T_{1\rho}$ has maximum values when *n*=2, and the values for NH_3 and CH_2 are 352 and 388 *ms*, respectively. The values when *n*=3 are 496 and 683 *ms*. In the case where *n*=4, the ^{1}H $T_{1\rho}$ value tends to increase gradually as the temperature increases. The three compounds show a similar tendency at temperatures below 350 K, but their values at temperatures above 350 K show different trends depending on the length of the carbon chain. It can be seen that the ^{1}H $T_{1\rho}$ values at high temperature are different according to the *n* value. In the case where *n*=3, there was no significant change in the vicinity of T_C, but in the case of *n*=4, it was

found to be slightly discontinuous in the vicinity of T_{C2}. The discontinuous changes of ^1H chemical shifts and ^1H $T_{1\rho}$ near T_{C2} are thought to be due to the rapid changes in the lattice constants *c* and *β*.[16]

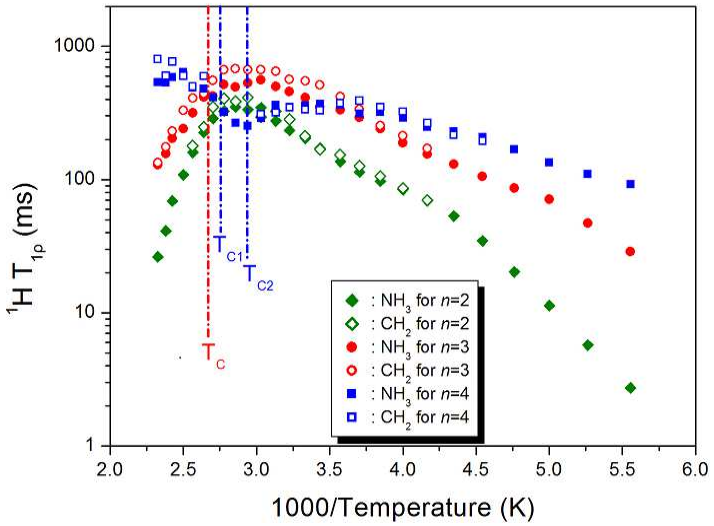

Figure 7. ^1H MAS NMR spin-lattice relaxation times $T_{1\rho}$ for CH_2 and NH_3 in $[NH_3(CH_2)_nNH_3]CdCl_4$ (*n*=2, 3, and 4) as a function of inverse temperature.

^{13}C MAS NMR

The ^{13}C MAS NMR chemical shifts for CH_2 in $[NH_3(CH_2)_nNH_3]CdCl_4$ were recorded at several temperatures. The signal for TMS reference was measured at 38.3 ppm at 300 K, and this value was set to 0 ppm for the ^{13}C chemical shift. Here, it is seen that CH_2-1 in the $[NH_3(CH_2)_nNH_3]$ cation is far from NH_3, and that CH_2-2 is located near NH_3. The results of ^{13}C chemical shifts according to the methylene chain length at 300 K are shown in the Supplementary Information. In the case where *n*=2, only one ^{13}C resonance line was obtained for CH_2-2. In the case where *n*=3 and 4, two ^{13}C resonance lines were obtained for CH_2-1 and CH_2-2, respectively. At 300 K, the ^{13}C chemical shift for *n*=2 was recorded at 37.36 ppm, and those for *n*=3 were observed at 25.00 and 39.09 ppm for CH_2-1 and CH_2-2, respectively. The ^{13}C chemical shifts for *n*=4 were observed at 25.30 and 42.85 ppm, respectively. Here, the chemical shifts for CH_2-1 are similar for these crystals, but those for CH_2-2 are different between *n*=2, 3, and 4. The full width at half maximum (FWHM) for ^{13}C NMR at 300 K are relatively narrow, ranging from 1.2 to 1.6 ppm.

Meanwhile, the chemical shifts for the in-situ ^{13}C MAS NMR spectra for the three compounds are shown in Fig. 8 with increasing temperature. In the case where *n*=2 (Fig. 8(a)), the ^{13}C chemical shifts for CH_2-2 increases slightly as the temperature increases. Some chemical shift changes around 290 K can also be seen. In case where *n*=3 (Fig. 8(b)), the slopes of the chemical shifts marked by red dotted lines are temperature dependent, with more variation for CH_2-2 than for CH_2-1. In addition, there was no

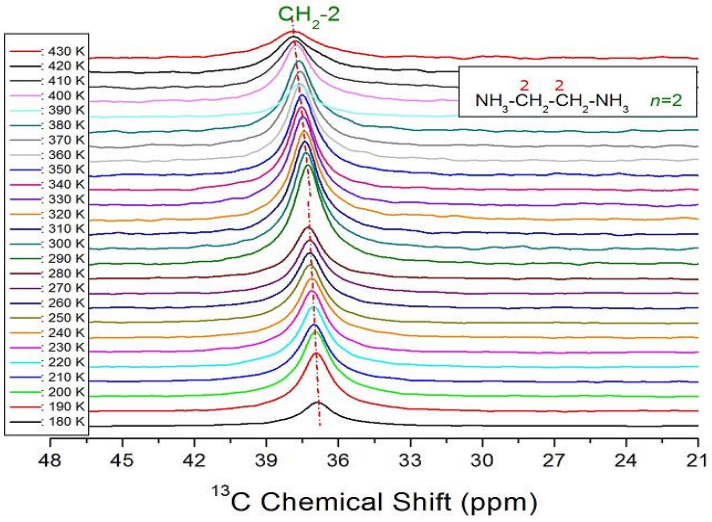

Figure 8(a). In-situ ^{13}C MAS NMR chemical shifts of $[NH_3(CH_2)_2NH_3]CdCl_4$, as a function of temperature.

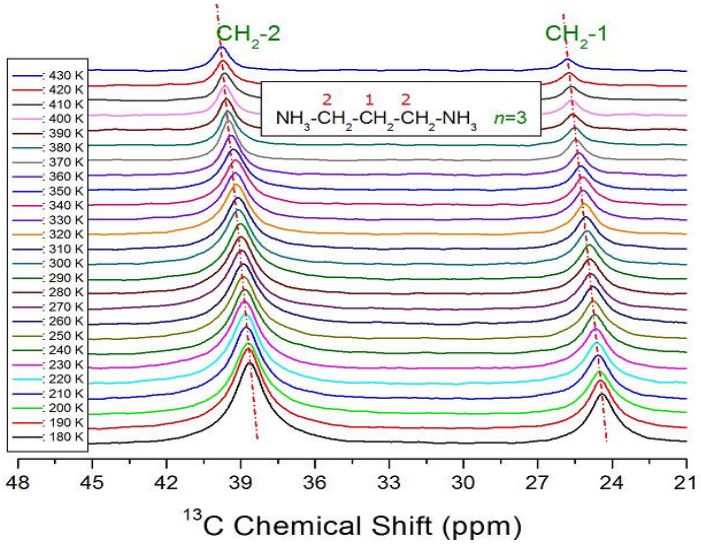

Figure 8(b). In-situ ^{13}C MAS NMR chemical shifts of $[NH_3(CH_2)_3NH_3]CdCl_4$, as a function of temperature.

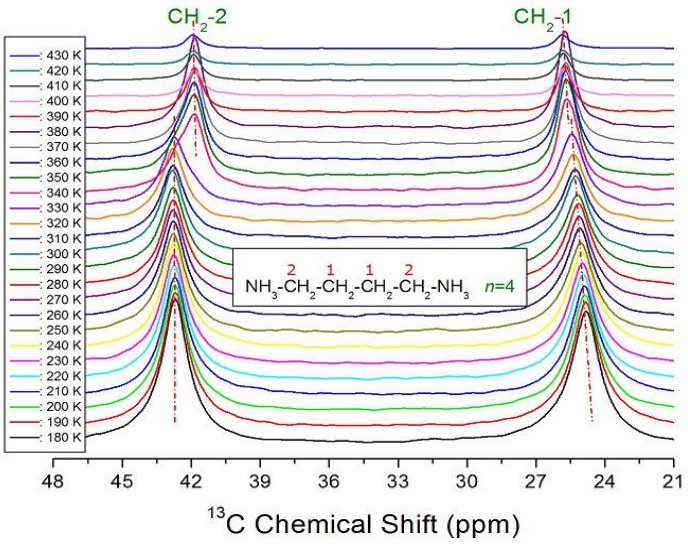

Figure 8(c). In-situ ^{13}C MAS NMR chemical shifts of $[NH_3(CH_2)_4NH_3]CdCl_4$, as a function of temperature.

change in chemical shifts near T_C. However, in the case where *n*=4 (Fig. 8(c)), the chemical shifts show discontinuity near T_{C2}, whereas they show continuity near T_{C1}. It can be seen that the chemical shifts of CH_2-2 near T_{C2} changes more than those of CH_2-1. In the three compounds, the chemical shifts of CH_2-2 (more so than that of CH_2-1) are thought to be affected by the N sites bonded to both ends of CH_2-2.

The ^{13}C MAS NMR spectrum showed a change in intensity with increasing delay time at each temperature. All these decay curves could be described by a single exponential function, and from the slope of their recovery traces, the ^{13}C $T_{1\rho}$ values for CH_2-1 and CH_2-2 were obtained for the three compounds and plotted as a function of 1000/T, as shown in Fig. 9. In the case where *n*=2, the ^{13}C $T_{1\rho}$ value first decreased slightly with increasing temperature and then decreased rapidly at higher temperatures. In the case where *n*=3, it decreased slightly with increase in temperature, then increased again, and finally decreased at temperatures above T_C. Meanwhile, the minimum $T_{1\rho}$ values (34.74 and 28.40 *ms* for CH_2-1 and CH_2-2, respectively) occur at 280 K. In the case where *n*=4, $T_{1\rho}$ decreases slightly as the temperature increases, and then increases rapidly near T_{C2}. Similar to that in the case of *n*=3, this tendency results from molecular motion below the phase transition temperature. There are distinct molecular motions, and the minimum $T_{1\rho}$ is due to the molecular motion of CH_2-1 and CH_2-2 in the $[NH_3(CH_2)_nNH_3]$ cations in the case where *n*=3 and 4, respectively. These $T_{1\rho}$ values could be described by the correlation time τ_C for the molecular motion, and the $T_{1\rho}$ value for the molecular motion is given by [36, 37]

$$T_{1\rho}^{-1} = C\,(\gamma_H^2 \gamma_C^2 \hbar^2 / r^6)[4f_a + f_b + 3f_c + 6f_d + 6f_e], \quad (2)$$

where $f_a = \tau_C/[1 + \omega_1^2\tau_C^2]$, $f_b = \tau_C/[1 + (\omega_H - \omega_C)^2\tau_C^2]$, $f_c = \tau_C/[1 + \omega_C^2\tau_C^2]$, $f_d = \tau_C/[1 + (\omega_H + \omega_C)^2\tau_C^2]$, and $f_e = \tau_C/[1 + \omega_H^2\tau_C^2]$. Here, C is a coefficient, γ_H and γ_C are the gyromagnetic ratios for ^1H and ^{13}C, respectively, $\hbar$ is the reduced Planck constant, *r* is the internuclear distance, ω_H and ω_C are the Larmor frequencies of ^1H and ^{13}C, respectively, and ω_1 is the frequency of the spin-lock field. Here, the ^{13}C $T_{1\rho}$ values were measured using the spin-locking pulse sequence with a locking pulse of ω_1=75.76 kHz for *n*=3 and ω_1=70.42 kHz for *n*=4. When $\omega_1\tau_C$=1, $T_{1\rho}$ has the minimum value. Therefore, a relationship between $T_{1\rho}$ and ω_1 was applied to obtain the coefficient C in Eq. (2). Using this coefficient, τ_C was calculated as a function of temperature. According to the Bloembergen-Purcell-Pound (BPP) theory, the local field fluctuation is governed by the thermal motion of CH_2-1 and CH_2-2. The correlation time τ_C for molecular motion at several temperatures follows the Arrhenius equation[33]

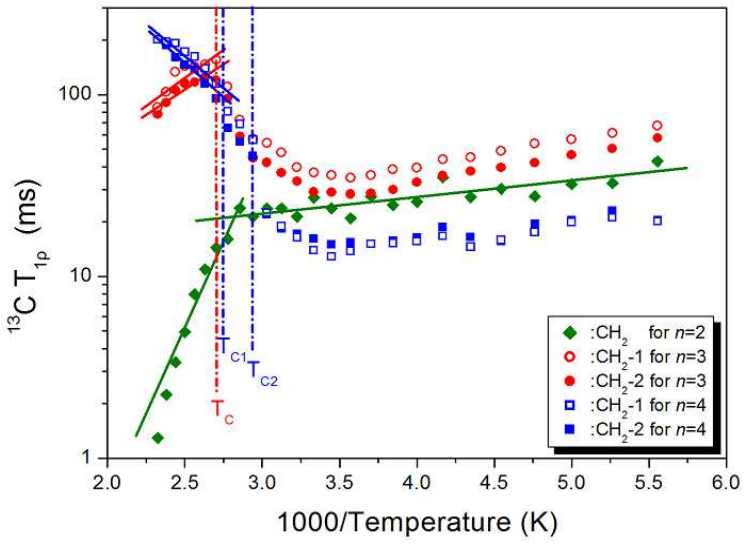

Figure 9. ^{13}C MAS NMR spin-lattice relaxation times $T_{1\rho}$ for CH_2-1 and CH_2-2 in $[NH_3(CH_2)_nNH_3]CdCl_4$ (*n*=2, 3, and 4) as a function of inverse temperature.

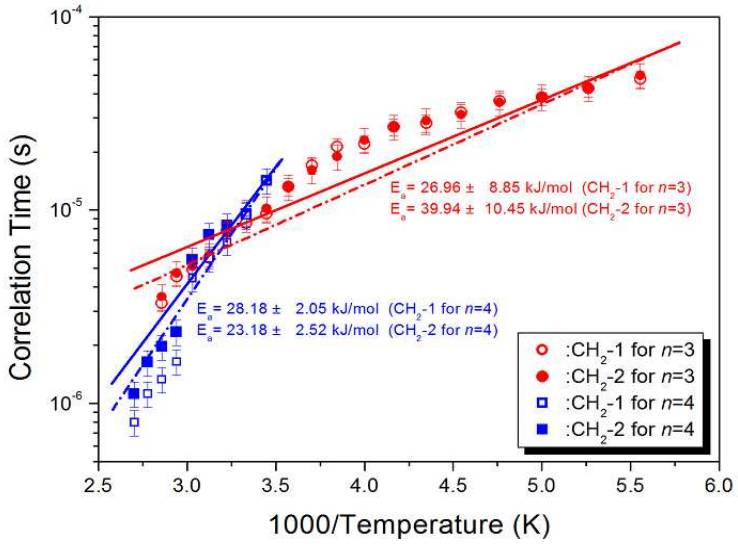

Figure 10. Arrhenius plots of the natural logarithm of the correlation times, τ_C, for ^{13}C in $[NH_3(CH_2)_3NH_3]CdCl_4$ and $[NH_3(CH_2)_4NH_3]CdCl_4$ as a function of inverse temperature.

$$\tau_C = \tau_o \exp(-E_a/k_BT) \quad (3)$$

where E_a and k_B are the activation energy of the motions and Boltzmann constant, respectively. The magnitude of E_a depends on the molecular dynamics. The plot of log τ_C vs. 1000/T provided the E_a values for CH_2-1 and CH_2-2, as shown in Fig. 10; in the case where *n*=3, the E_a values of CH_2-1 and CH_2-2 below T_C were 26.96 ± 8.85 and 39.94 ± 10.45 kJ/mol, respectively. When *n*=4, the E_a values of CH_2-1 and CH_2-2 below T_{C2} were 28.18 ± 2.05 and 23.18 ± 2.51 kJ/mol, respectively. Additionally, above T_C when *n*=3, the E_a values for CH_2-1 and CH_2-2 were 10.18 ± 2.68 and 8.45 ± 2.04 kJ/mol, respectively. Unlike that in the cases of *n*=2 and 3, the trend of ^{13}C $T_{1\rho}$ at high temperatures is very different for *n*=4. Above T_{C1}, they were 13.42 ± 2.01 and 14.35 ± 1.41 kJ/mol, respectively. When *n*=3 and 4, the E_a values at low temperatures are greater than that at high temperatures, whereas when *n*=2, their results are opposite (1.70 ± 0.24 kJ/mol below 330 K and 35.19 ± 4.32 kJ/mol above 330 K).

Static ^{14}N NMR

Static ^{14}N NMR investigations of $[NH_3(CH_2)_nNH_3]CdCl_4$ single crystals were conducted over the temperature range of 180–430 K. The ^{14}N spectra were obtained using the solid-state echo method by static NMR. Two ^{14}N NMR signals were expected from the quadrupole interactions due to the spin number I=1.[38] The ^{14}N NMR spectrum for *n*=2, 3, and 4 differed with increasing temperature, as shown in Fig. 11. Here, the measurements were performed by keeping the *c*-axis of the single crystals parallel to the direction of the magnetic field. In the case of *n*=2, the two resonance lines of one pair decreased with increasing temperature, then decreased to a minimum near 400 K, and then increased again. In the case of *n*=3, the chemical shifts for six resonance lines due to the three pairs caused a large change near T_C. The symbols with the same color below T_C indicate the same pairs for ^{14}N. Near 374 K (=T_C), the number of resonance lines and chemical shifts of the NMR spectrum showed abrupt changes; three pairs turned into just two pairs. The changes in the ^{14}N chemical shift as a function of temperature were attributed to the variations in the structural geometry. In addition, the chemical shifts of the ^{14}N signals below T_C changed almost continuously, and the chemical shifts for ^{14}N above T_C remained constant with temperature. The ^{14}N NMR spectrum exhibits a reduction in the NMR lines from three to two pairs of lines at the phase transition T_C. Finally, when *n*=4, the four resonance lines due to two inequivalent N sites showed no change in temperature below T_{C2}; however, it was difficult to detect because the line width suddenly increased above T_{C2}. In the cases of *n*=3 and 4, the different N spectra were explained as follows. None of the previously reported X-ray results[6, 16, 24, 27] include different N sites; therefore, two or three different N sites are thought to have a twin domain due to the ferroelastic property in materials with the organic–inorganic perovskite structure reported recently.

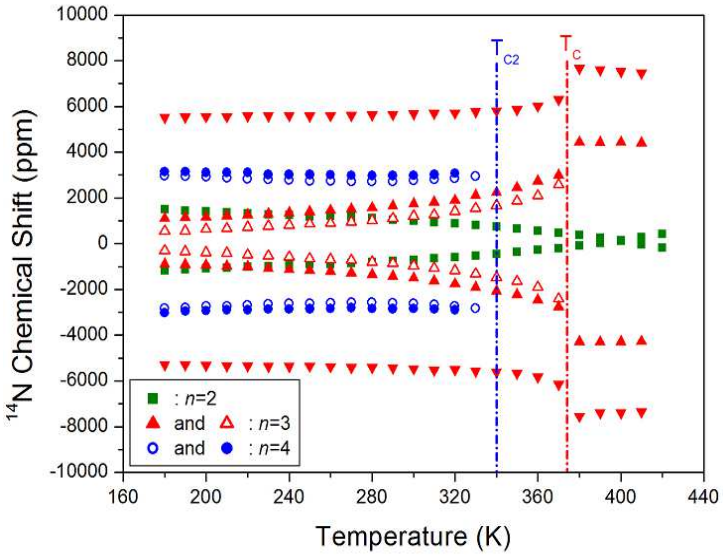

Figure 11. Static ^{14}N NMR chemical shifts of $[NH_3(CH_2)_nNH_3]CdCl_4$ (n=2, 3, and 4) as a function of temperature.

^{113}Cd MAS NMR

^{113}Cd MAS NMR experiments were performed to examine the structural dynamics in the anions of $[NH_3(CH_2)_nNH_3]CdCl_4$ single crystals. ^{113}Cd has an isotopic abundance of 12.3% and a spin of I=1/2. ^{113}Cd NMR spectroscopy has been used to examine the structure and dynamics of various inorganic and organic materials. The ^{113}Cd MAS NMR spectra for the three crystals were obtained as a function of temperature, as shown in Fig. 12. The chemical shifts are related to the local field at the position of the resonating nucleus in the crystals.[39] The ^{113}Cd chemical shifts for the three crystals shift slightly in the negative direction as the temperature increases. However, in the case where n=4, it was discontinuous near T_{C2}. This result suggests that in the cases when n=2 and 3, there is no significant change in the environment near Cd depending on the temperature, whereas in the case of n=4, the environment around Cd changes near the phase transition temperature. In addition, the difference in Cd chemical shifts for the three materials seems to be due to the difference in the Cd–Cl distance as shown in Table 1. In other words, it is consistent that the Cd–Cl distance increases as the n value increases. Similarly, the change in the chemical shift near T_{C2} is attributed to the shortening of the Cd–Cl distance from the average 2.646 Å to 2.6198 Å.[16]

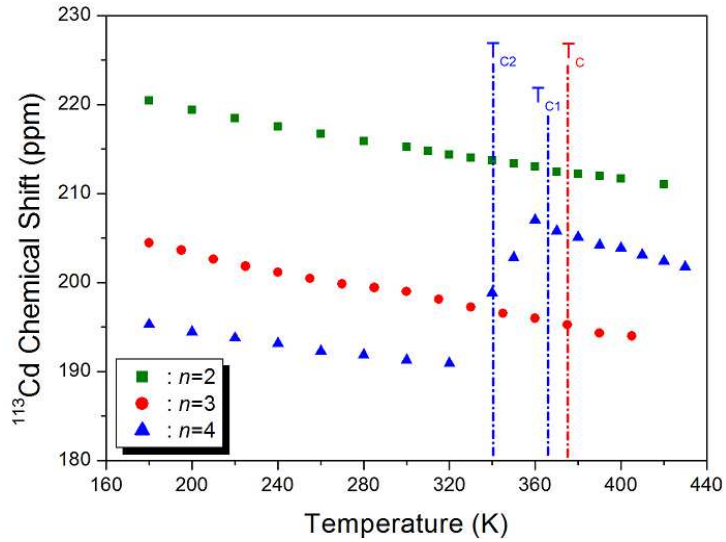

Figure 12. ^{113}Cd MAS NMR chemical shifts of $[NH_3(CH_2)_nNH_3]CdCl_4$ (n=2, 3, and 4) as a function of temperature.

The ^{113}Cd MAS NMR spectrum for three crystals measured the change in intensity with various delay times at 300 K. The decay curves were described by a single exponential function, and the ^{113}Cd $T_{1\rho}$ values were obtained from the slope of their recovery traces. In the cases where *n*=2, 3, and 4, the $T_{1\rho}$ values were 2058, 1512, and 1101 *ms*, respectively. All the $T_{1\rho}$ values for ^{1}H, ^{13}C, and ^{113}Cd at 300 K are listed in Table 2. ^{113}Cd $T_{1\rho}$ was very long compared to ^{1}H $T_{1\rho}$ and ^{13}C $T_{1\rho}$. The long ^{113}Cd $T_{1\rho}$ values with *n*=2 at 300 K were considered to be more rigid than the others (*n*=3 and 4) because the Cd-Cl length is short as shown in Table 1; a longer $T_{1\rho}$ indicates that the transfer of energy from the nuclear spin system to the surrounding environment is not very easy.

Table 2. The spin-lattice relaxation times, $T_{1\rho}$ values for ^{1}H, ^{13}C, and ^{113}Cd of $[NH_3(CH_2)_nNH_3]CdCl_4$ (*n*=2, 3, and 4) at 300 K.

	^{1}H $T_{1\rho}$ (*ms*)	^{13}C $T_{1\rho}$ (*ms*)	^{113}Cd $T_{1\rho}$ (*ms*)
n=2	204.20 (NH_3)		2058
	211.92 (CH_2)	27.67 (CH_2-2)	
n=3	411.53 (NH_3)	37.13 (CH_2-1)	1512
	551.12 (CH_2)	29.13 (CH_2-2)	
n=4	334.98 (NH_3)	14.06 (CH_2-1)	1101
	357.83 (CH_2)	13.90 (CH_2-2)	

Discussion

The structures and phase transition temperatures for $[NH_3(CH_2)_nNH_3]CdCl_4$ (*n*=2, 3, and 4) crystals were confirmed by X- ray diffraction and DSC experiments. The thermal stability improved as the length of the carbon chains in the $[NH_3(CH_2)_nNH_3]$ cations increased. In addition, based on the information obtained from NMR studies on methylene chain length, the structural dynamics of the $[NH_3(CH_2)_nNH_3]$ cation and $CdCl_6$ anion in $[NH_3(CH_2)_nNH_3]CdCl_4$ crystals were analyzed. ^{1}H, ^{13}C, ^{14}N, and ^{113}Cd NMR were considered by determining the changes in the chemical shifts accompanying a change in the crystallographic environment. When *n*=2, the ^{1}H, ^{13}C, and ^{113}Cd chemical shifts hardly change with temperature, indicating that there is no phase transition phenomenon. When *n*=3, ^{1}H, ^{13}C, and ^{113}Cd chemical shifts exhibit a continuous change near T_C, indicating that the crystal structure is orthorhombic at both low and high temperatures, and the lattice constant hardly changes. Finally, when *n*=4, the ^{1}H, ^{13}C, and ^{113}Cd chemical shifts are continuous near T_{C1}, but discontinuous around T_{C2}. This is attributed to a large change in the lattice parameters *c* and *β* near T_{C2}.

The molecular dynamics near the phase transition temperatures were analyzed in terms of the $T_{1\rho}$ values for ^{1}H and ^{13}C. ^{1}H and ^{13}C $T_{1\rho}$ are almost continuous when *n*=2 and 3, but when *n*=4, they show a discontinuity near T_{C2}, as with the chemical shifts. Overall, *n*=2 and 3 showed a rapid decrease in $T_{1\rho}$ of ^{1}H and ^{13}C at high temperatures, whereas *n*=4 showed an increase at high temperatures. The short ^{13}C $T_{1\rho}$ values at low temperatures in the case of *n*=4 were considered to be more flexible than the others because the N–C–C–C–C–N lengths are long.

Conclusion

The crystal structures were found to be monoclinic when *n* was even and orthorhombic when *n* was odd, but there were little differences in thermal and physical properties. The difference in molecular motion according to the length of the cation was observed only at high temperatures. In the $[NH_3(CH_2)_nNH_3]$ cations, ^{13}C $T_{1\rho}$ with *n*=4 at low temperature has shorter values than those with *n*=2 and 3. It was found that as the carbon length increased, it became more flexible. Overall, ^{113}Cd $T_{1\rho}$ at 300 K is very long compared to the ^{1}H and ^{13}C $T_{1\rho}$ values. This is thought to be related to the Cd-Cl bond length. These results provide insight into the thermal stability and molecular dynamics of $[NH_3(CH_2)_nNH_3]CdCl_4$ (*n*=2, 3, and 4) crystals as a function of the length of CH_2 groups in the carbon chain and are expected to facilitate future research as well as potential applications in supercapacitors, batteries, and fuel cells.

References

1. Pradeesh, K.; Baumberg, J. J.; Vijaya Prakash, G. Exciton switching and peierls transitions in hybrid inorganic-organic self-assembled quantum wells, *Appl. Phys. Lett*. **95**, 173305 (2009).
2. Cheng, Z.; Lin, J. Layered organic-inorganic hybrid perovskites: structure, optical properties, film preparation, patterning and templating engineering, *Cryst. Eng. Com*. **12**, 2646 (2010).
3. Pradeesh, K.; Yadav, G. S.; Singh, M.; Vijaya Prakash, G. Synthesis, structure and optical studies of inorganic-organic hybrid semiconductor, $NH_3(CH_2)_{12}NH_3PbI_4$, *Mater. Chem. Phys*. **124**, 44 (2010).
4. Saikumar, S.; Ahmad, J. J.; Baumberg, G.; Vijaya Prakash, G. Fabrication of excitonic luminescent inorganic-organic hybrid nano- and microcrystals. *Scr. Mater*. **67**, 834 (2012).
5. Staskiewicz, B.; Czupinski, O.; Czapla, Z. On some spectroscopic properties of a layered 1,3-diammoniumpropylene tetrabromocadmate hybrid crystal. *J. Mol. Struct.* **1074**, 723 (2014).
6. Staskieqicz, B.; Turowska-Tyrk, I.; Baran, J.; Gorecki, Cz.; Czapla, Z. Structural characterization, thermal, vibrational properties and molecular motions in perovskite-type diamonopropanetetrachlorocadmate $NH_3(CH_2)_3NH_3CdCl_4$ crystal. *J. Phys. Chem. Solids* **75**, 1305 (2014).
7. Ahmad, S.; Hanmandlu, C.; Kanaujia, P. K.; Vijaya Prakash, G. Direct deposition strategy for highly ordered inorganic organic perovskite thin films and their optoelectric applications, *Opt. Mater Express* **4**, 1313 (2014).
8. Gonzalez-Carrero, S.; Galian, R. E.; Perez-Prieto, J. Organometa halide perovskites: bulk low-dimension materials and nanoparticles, *Part. Syst. Charact*. **32**, 709 (2015).
9. Czapla, Z.; Przeslawski, J.; Crofton, M.; Janczak, J.; Czupinski, O.; Ingram, A.; Kostrzewa, M. Structural phase trasition in a perovskite-type $NH_3(CH_2)_3NH_3CuCl_4$ crystal X-ray and optical studies. *Phase Transitions* **90**, 637 (2017).
10. Abdel-Adal, S. K.; Kocher-Oberlehner, G.; Ionov, A.; Mozhchil, R. N. Effect of organic chain length on structure, electronic composition, lattice potential energy, and optical properties of 2D hybrid perovskites $[(NH_3)(CH_2)_n(NH_3)]CuCl_4$, n = 2-9. *Appl. Phys*. A **123**, 531 (2017).
11. Sourisseau, C.; Lucazeau, G.; Dianoux, A. J. Neutron scattering study of the reorientational motions for NH_3 groups in $(NH_3(CH_2)_3NH_3)MnCl_4$. *J. Physique* **44**, 967 (1983).
12. Chhor, K.; Bocquet, J. F.; Pommier, C. Low-temperature adiabatic calorimeter with an automatic data-acquisition system for the temperature range 10 to 310 K. The molar heat capacity of $NH_3(CH_2)_3NH_3MnCl_4$. *J. Chem. Thermodynamics* **17**, 379 (1985).
13. Eremenko, V. V.; Fomin, V. I.; Kurnosov, V. S. Spin wave spectrum of quasi-two-dimensional antiferromagnet $NH_3(CH_2)_2NH_3MnCl_4$. *Physica* B **194-196**, 187 (1994).
14. Bissey, J.-C.; Filloleau, N.; Chanh, N.-B.; Berger, R.; Flandrois, S. Exchange interaction as studied by EPR in a two-dimensional molecular composite $[NH_3\text{-}(CH_2)_4\text{-}NH_3]MnCl_4$. *Solid State Commun*. **106**, 385 (1998).
15. Bogdan, M. M.; Kobets, M. I.; Khats'ko, E. N. Chaotic regimes of antiferromagnetic resonance in a quasi-two-dimensional easy-axis antiferromagnet $(NH_3)_2(CH_2)_4MnCl_4$. *Low. Temp*. **25**, 192 (1999).
16. Khechoubi, M.; Bendani, A.; Chnh, N. B.; Courseille, C.; Duplessix, R.; Couzi, M. Thermal conformational changes in a bidimensional molecular composite material: a thermodynamic and crystallographic study of $NH_3\text{-}(CH_2)_4\text{-}NH_3CdCl_4$, *J. Phys. Chem. Solids* **55**, 1277-1288 (1994).
17. Niang, A.; Ablart, G.; Pescia, J.; Khechoubi, E. M.; Chanh, N. B.; Duplessix, R. Electron-spin dynamics in the two-dimensional compound $[NH_3(CH_2)_4NH_3]MnCl_4$. *Phys. Stat. Sol*. (b) **178**, 477 (1993).
18. Yadav, R.; Swain, D.; Kundu, P. P.; Nair, H. S.; Narayana, C.; Elizabeth, S. Dielectric and Raman investigations of structural phase transitions in $(C_2H_5NH_3)CdCl_4$. *Phys. Chem. Chem. Phys*. **17**, 12207 (2015).
19. Elseman, M.; Shalan, A. E.; Sajid, S.; Rashad, M. M.; Hassan, A. M.; Li, M. Copper-substituted lead perovskite materials constructed with different halides for working $(CH_3NH_3)_2CuX_4$-based perovskite solar cells from experimental and theoretical view. *ACS Appl. Mater. Interfaces* **10**, 11699 (2018).
20. Aramburu, J. A.; Garcia-Fernandez, P.; Mathiesen, N. R.; Garcia-Lastra, J. M.; Moreno, M. Changing the usual interpretation of the structure and ground state of Cu^{2+} layered perovskites. *J. Phys. Chem*. C **122**, 5071 (2018).
21. Al-Amri, A. M.; Leung, S.-F.; Vaseem, M.; Shamin, A.; He, J.-H. Fully inkejet-printed photodetector using a grapheme/perovskite/grapheme heterostructure. *IEEE Trans. Electron Dev.* **66**, 2657 (2019).
22. Al-Amri, A. M.; Cheng, B.; He, J.-H. Perovskite methylammonium lead trihalide heterostructures: progress and challenges. IEEE Trans. *Nanotechnol*. **18**, 1 (2019).

23. Lin, C.-H.; Kang, C.-Y.; Wu, T.-Z.; Tsai, C.-L.; Sher, C.-W.; Guan, X.; Lee, P.-T.; Wu, T.; Ho, C.-H.; Kuo, H. C.; He, J.-H. Giant optical anisotropy of perovskite nanowire array films. *Adv. Funct. Mater*. **30**, 1909275 (2020).
24. Battaglia, L. P.; Bonamartini-Corradi, A.; Pelosi, G.; Cramarossa, M. R.; Manfredini, T.; Pellacani, G. C.; Motori, A.; Saccani, A.; Sandrolini, F.; Brigatti, M. F. Synthesis and characterization of layered chlorocadmates (II) with perovskite-like structures. *Chem. Mater* **4**, 813 (1992).
25. Lamhamdi, A.; Mejdoubi, E.; Fejfarova, K.; Dusek, M.; Bali, B. E. Poly[ethane-1,2-diammonium tetra-μ-chlorido-cadmate (II)]. *Acta Cryst*. E **65**, m215-216 (2009).
26. Willett, R. D. Propylenediammonium tetrachlorocadmate (II), *Acta Cryst*. B **33**, 1641-1643 (1977).
27. Kind, R.; Plesko, S.; Gunter, P.; Ross, J.; Fousek, J. Structural phase transitions in the perovskite-type layer compounds $NH_3(CH_2)_3NH_3CdCl_4$, $NH_3(CH_2)_4NH_3MnCl_4$, and $NH_3(CH_2)_5NH_3CdCl_4$. *Phys. Rev*. B **23**, 5301 (1981).
28. Lim, A. R. Thermal property, structural characterization, and physical property of cation and anion in organic-inorganic perovskite $[(CH_2)_3(NH_2)_2]CdCl_4$ crystal. *J. Solid State Chem*. **295**, 121909 (2021).
29. Feki, H.; Bahri, M.; Maalej, A.; Abid, Y.; Jaidane, N.; Lakhdar, Z. B. Conformational calculation and phase transitions in NH_3-$(CH_2)_4$-NH_4CdCl_4, *Phase Transitions* **72**, 331-340 (2000).
30. Lim, A.R.; Kim, S.H.; Joo, Y.L. Physicochemical properties and structural dynamics of organic-inorganic hybrid $[NH_3(CH_2)_3NH_3]Zn\mathit{X}_4$ (*X*=Cl and Br) crystals, *Scientific Reports* **11**, 8408-8416 (2021).
31. Lim, A.R. Thermodynamic properties, structural characteristics, and cation dynamics of perovskite-type layer crystal $[NH_3(CH_2)_2NH_3]ZnCl_4$, *ACS Omega* **5**, 31417-31422 (2020).
32. Yoon, M.B.; Lee, W.J.; Lim, A.R. Thermal property and structural molecular dynamics of organic-inorganic hybrid perovskite 1,4-butanediammonium tetrachlorocuprate, *RSC Advances* **10**, 34800-34805 (2020).
33. Abragam, A. *The Principles of Nuclear Magnetism* (Oxford University press, 1961).
34. Harris, R.K. *Nuclear Magnetic Resonance Spectroscopy* (Pitman Pub., UK, 1983).
35. Koenig, J. L. *Spectroscopy of Polymers* (Elsevier, New York, 1999).
36. Bloembergen, N.; Purcell, E. M.; Pound, R. V. Relaxation effects in nuclear magnetic resonance absorption. *Phys. Rev*. **73**, 679 (1948).
37. Lim, A. R.; Shin, H. K. ^{1}H and ^{7}Li nuclear magnetic resonance study of the superionic crystals $K_4LiH_3(SO_4)_4$ and $(NH_4)_4LiH_3(SO_4)_4$. *J. Appl. Phys*. **107**, 63513 (2010).
38. Mulla-Osman, S.; Michel, D.; Czapla, Z. ^{14}N NMR study of the domain structure of tetramethyl-ammonium cadmium chloride (TMCC), *Phys. Stat. Sol.* (b) **236**, 173-181 (2003).
39. Sakida, S.; Kawamoto, Y. ^{113}Cd MAS and static NMR study of halogenocadmate crystals, *J.Phys. Chem. Solids* **63**, 151 (2002).

Acknowledgments

This research was supported by the Basic Science Research program through the National Research Foundation of Korea (NRF), funded by the Ministry of Education, Science, and Technology (2018R1D1A1B07041593 and 2016R1A6A1A03012069).

Author contributions

A.R.L. designed the project, performed NMR experiments, and wrote the manuscript.

Competing of interests

The authors declare no competing interests.

Additional information

Supplementary information is available for this paper

Correspondence and request for materials should be addressed to A.R. L.

Figures

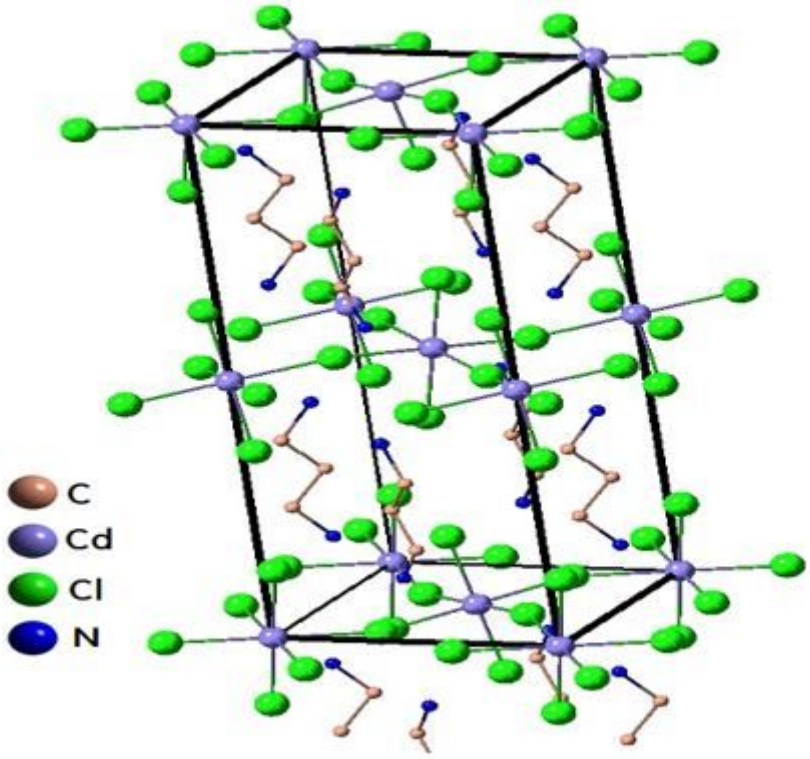

Figure 1

The structure of [NH3(CH2)3NH3]CdCl4 crystal at room temperature.

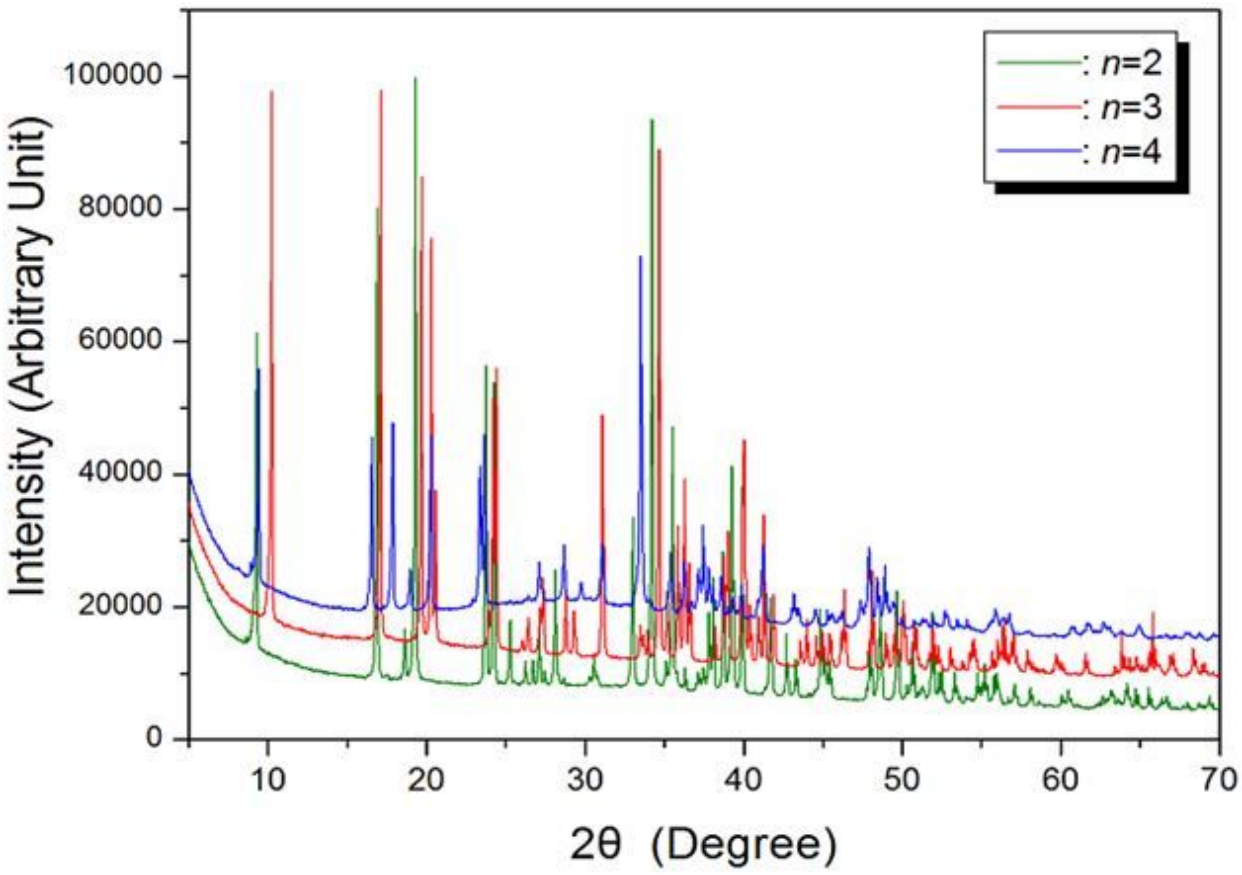

Figure 2

X-ray diffraction patterns of [NH3(CH2)nNH3]CdCl4 (n=2, 3, and 4) at 298 K.

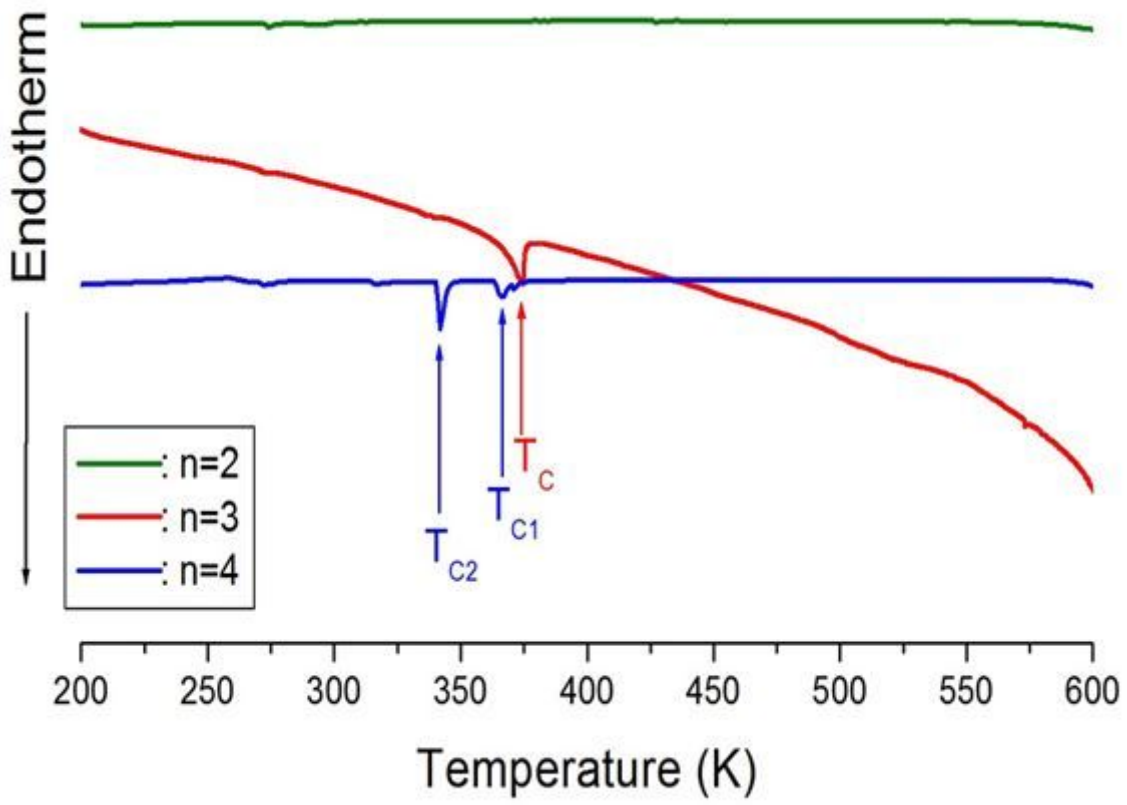

Figure 3

Differential scanning calorimetry (DSC) curves of [NH3(CH2)nNH3]CdCl4 (n=2, 3, and 4).

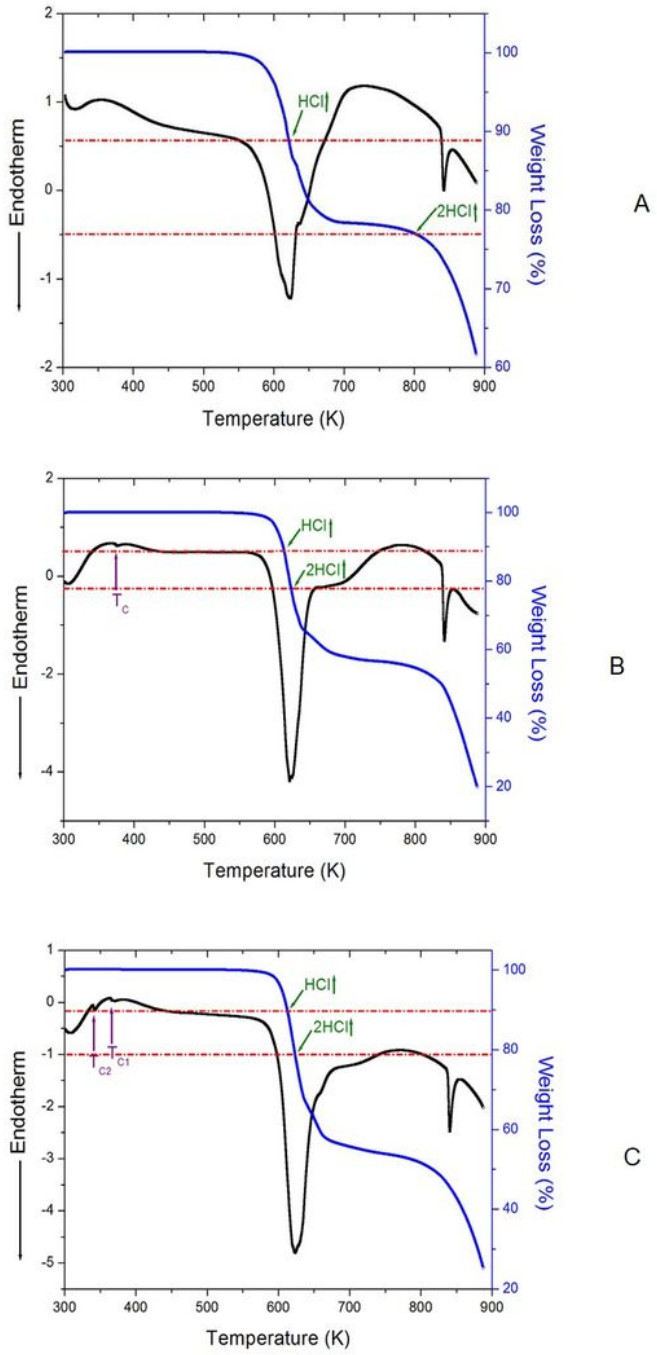

Figure 4

(a). Thermogravimetric analysis (TGA) and differential thermal analysis (DTA) results of [NH3(CH2)2NH3]CdCl4. (b). Thermogravimetric analysis (TGA) and differential thermal analysis (DTA) results of [NH3(CH2)3NH3]CdCl4. (c). Thermogravimetric analysis (TGA) and differential thermal analysis (DTA) results of [NH3(CH2)4NH3]CdCl4.

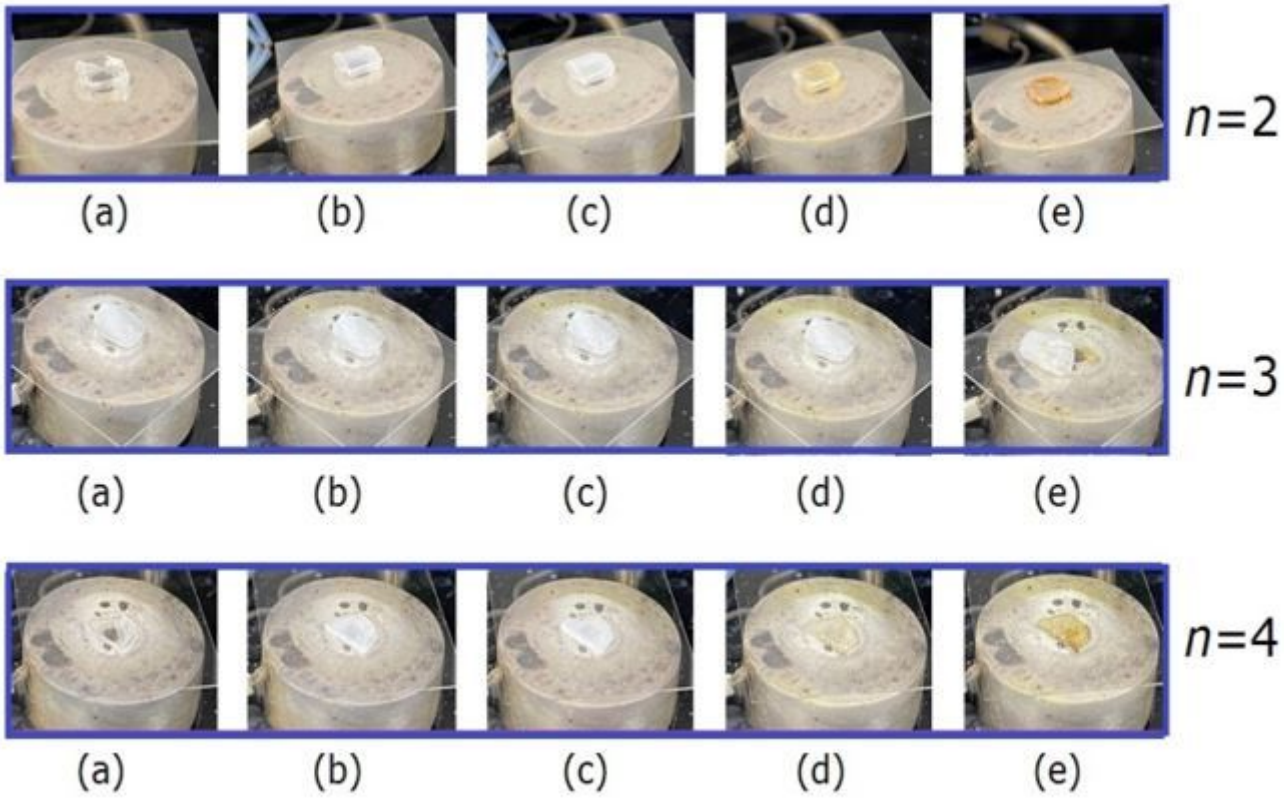

Figure 5

Changes in crystal by optical polarizing microscopy at (a) 300 K, (b) 547 K, (c) 573 K, (d) 622 K, and (e) 633 K for [NH3(CH2)2NH3]CdCl4 with n=2; (a) 296 K, (b) 563 K, (c) 613 K, (d) 653 K, (e) 673 K for [NH3(CH2)3NH3]CdCl4 with n=3; and (a) 295 K, (b) 353 K, (c) 573 K, (d) 659 K, (e) 670 K for [NH3(CH2)4NH3]CdCl4 with n=4.

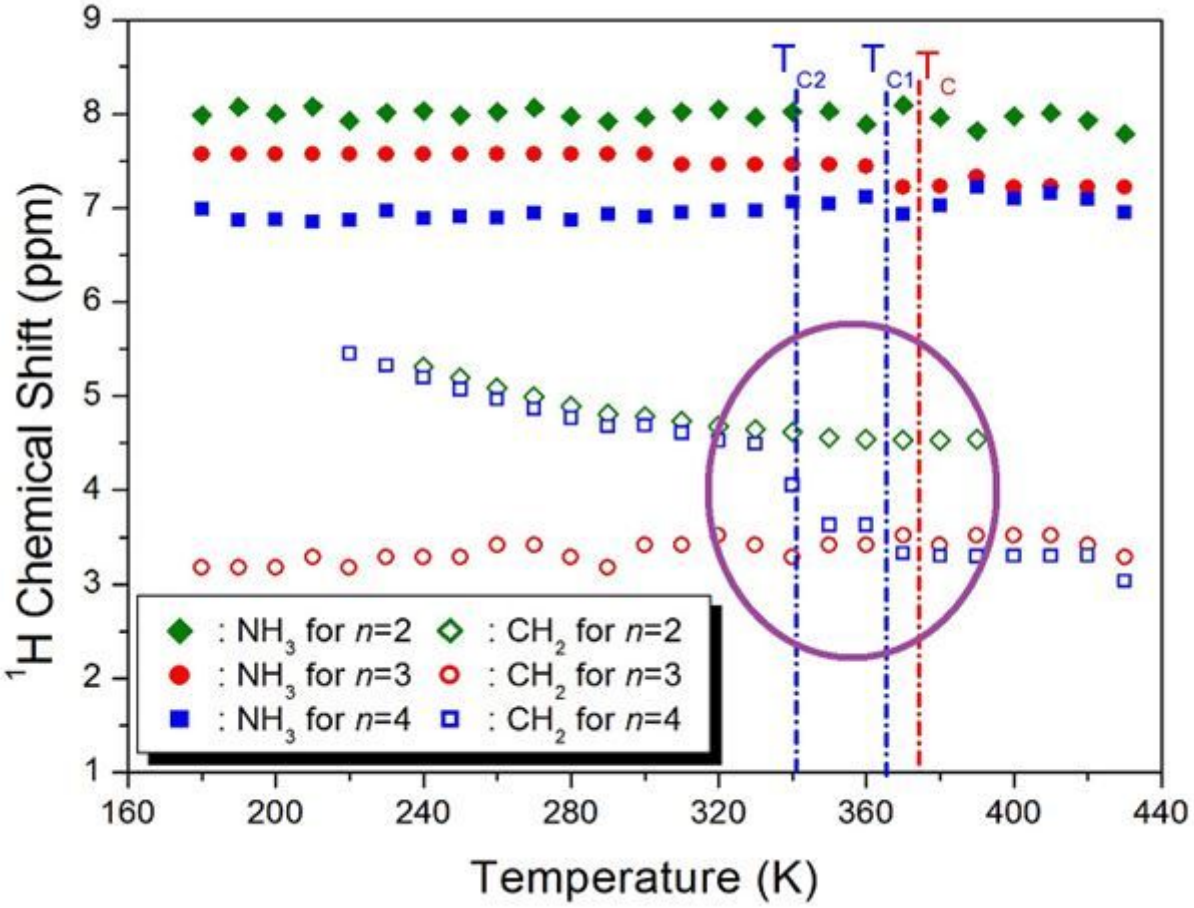

Figure 6

1H NMR chemical shifts for NH3 and CH2 in [NH3(CH2)nNH3]CdCl4 (n=2, 3, and 4) as a function of temperature.

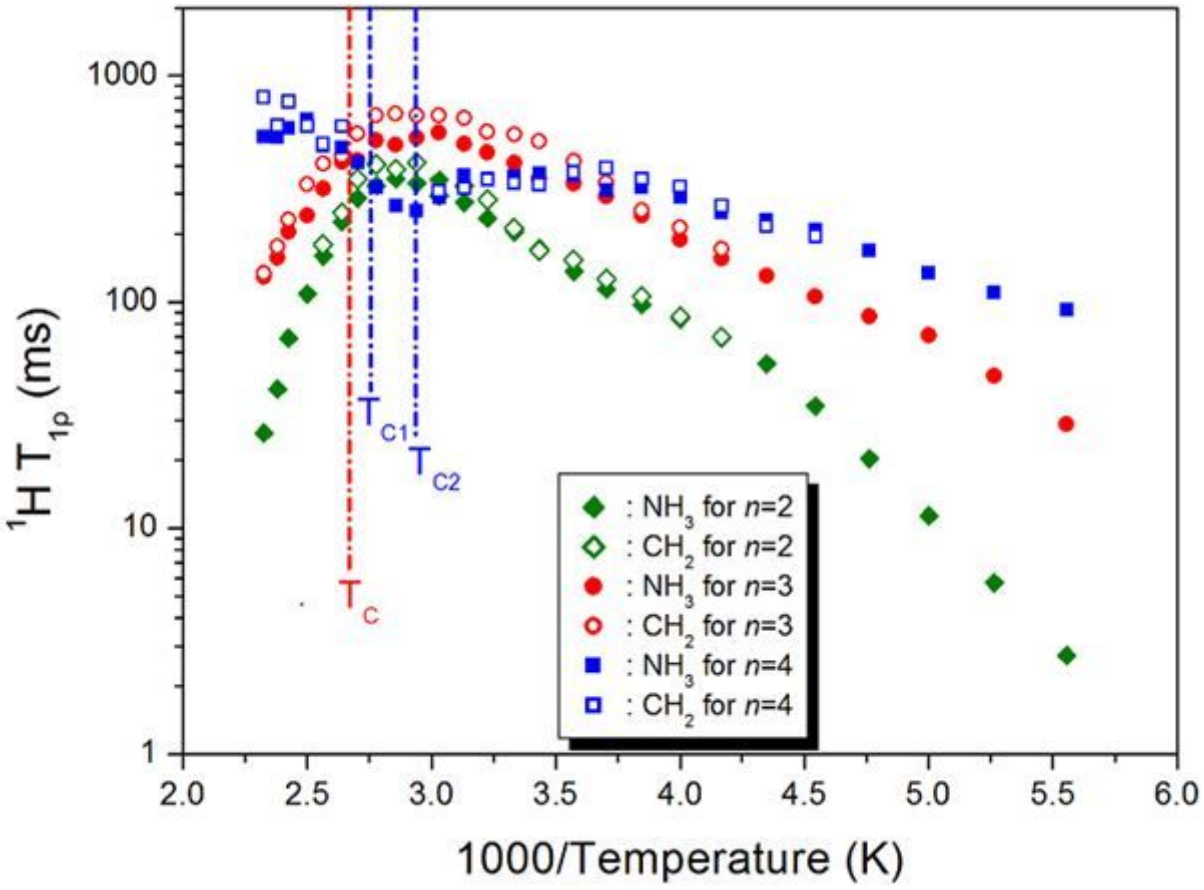

Figure 7

1H MAS NMR spin-lattice relaxation times T1ρ for CH2 and NH3 in [NH3(CH2)nNH3]CdCl4 (n=2, 3, and 4) as a function of inverse temperature.

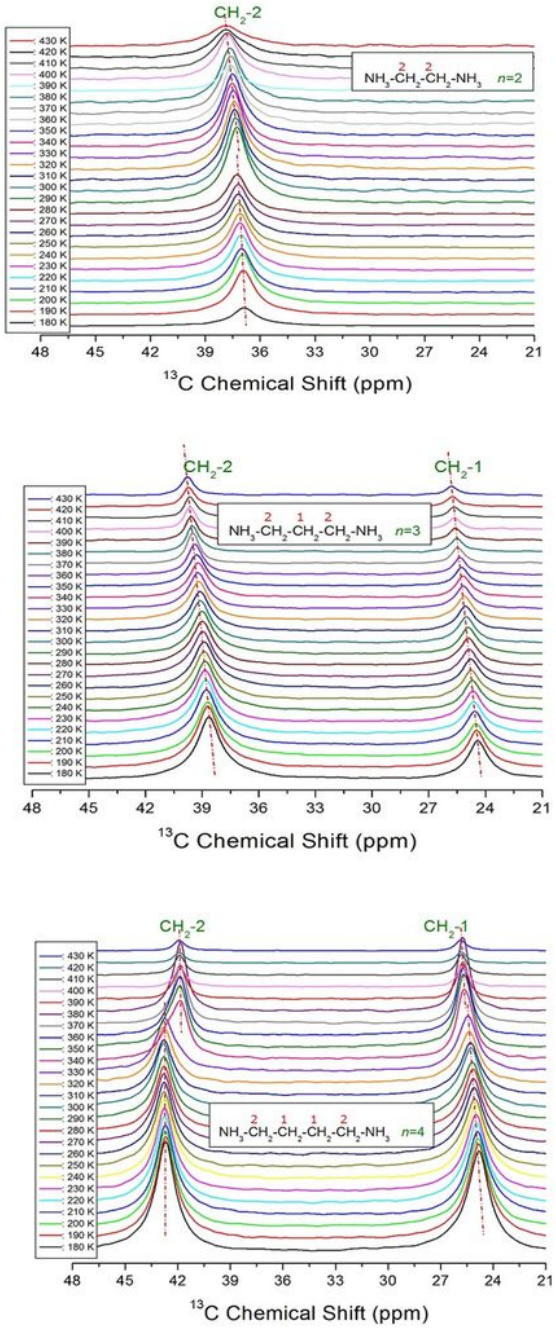

Figure 8

(a). In-situ 13C MAS NMR chemical shifts of [NH3(CH2)2NH3]CdCl4, as a function of temperature. b). In-situ 13C MAS NMR chemical shifts of [NH3(CH2)3NH3]CdCl4, as a function of temperature. (c). In-situ 13C MAS NMR chemical shifts of [NH3(CH2)4NH3]CdCl4, as a function of temperature.

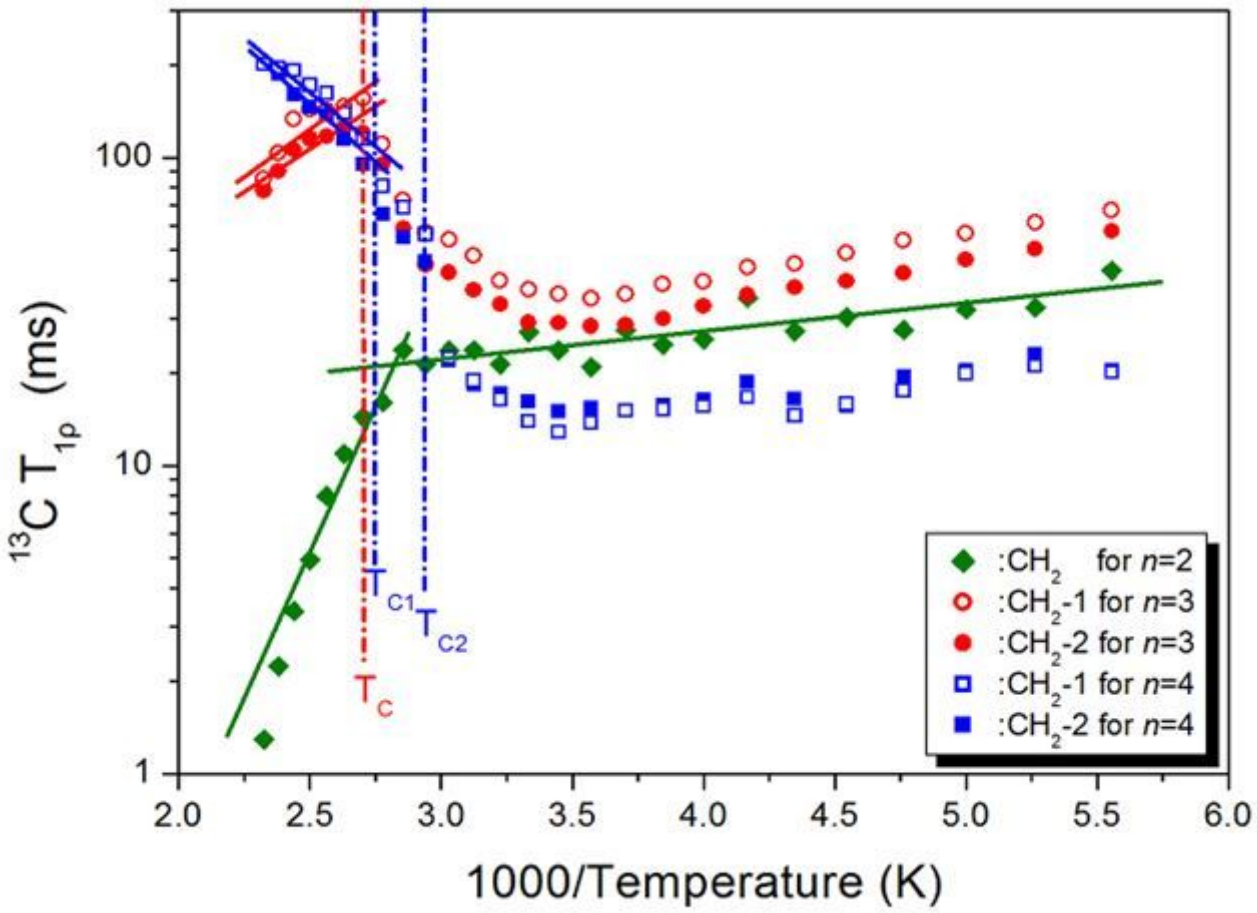

Figure 9

13C MAS NMR spin-lattice relaxation times T1ρ for CH2-1 and CH2-2 in [NH3(CH2)nNH3]CdCl4 (n=2, 3, and 4) as a function of inverse temperature.

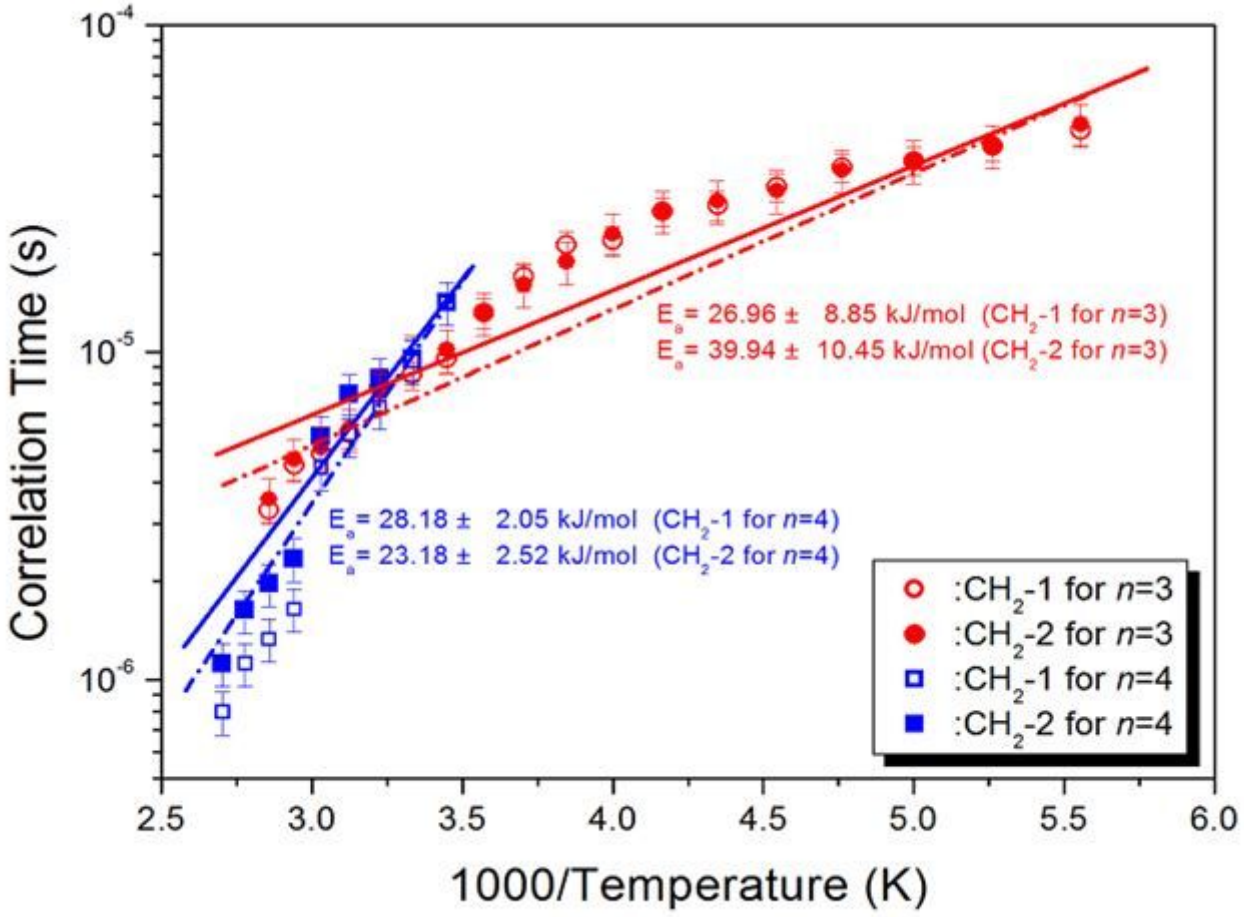

Figure 10

Arrhenius plots of the natural logarithm of the correlation times, τC, for 13C in [NH3(CH2)3NH3]CdCl4 and [NH3(CH2)4NH3]CdCl4 as a function of inverse temperature.

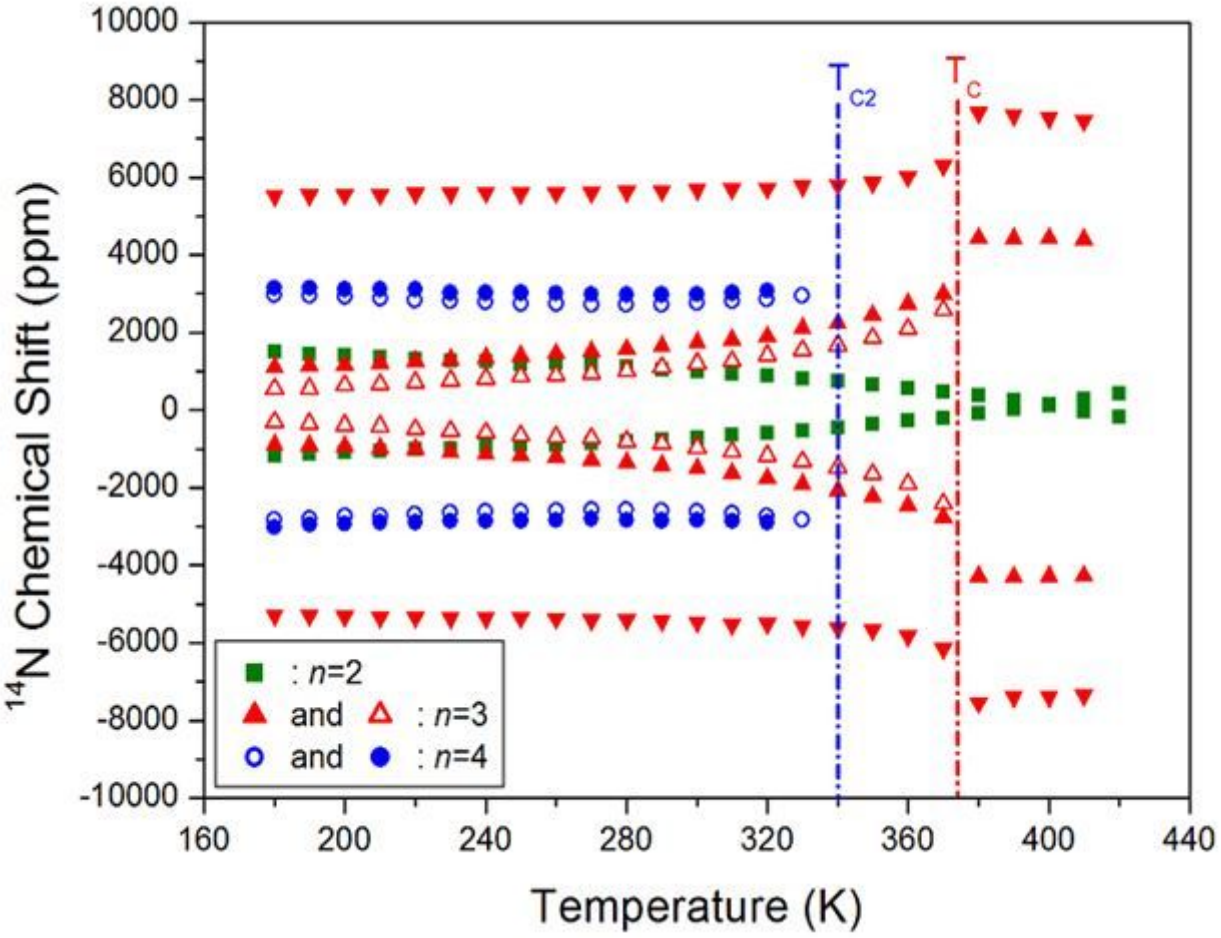

Figure 11

Static 14N NMR chemical shifts of [NH3(CH2)nNH3]CdCl4 (n=2, 3, and 4) as a function of temperature.

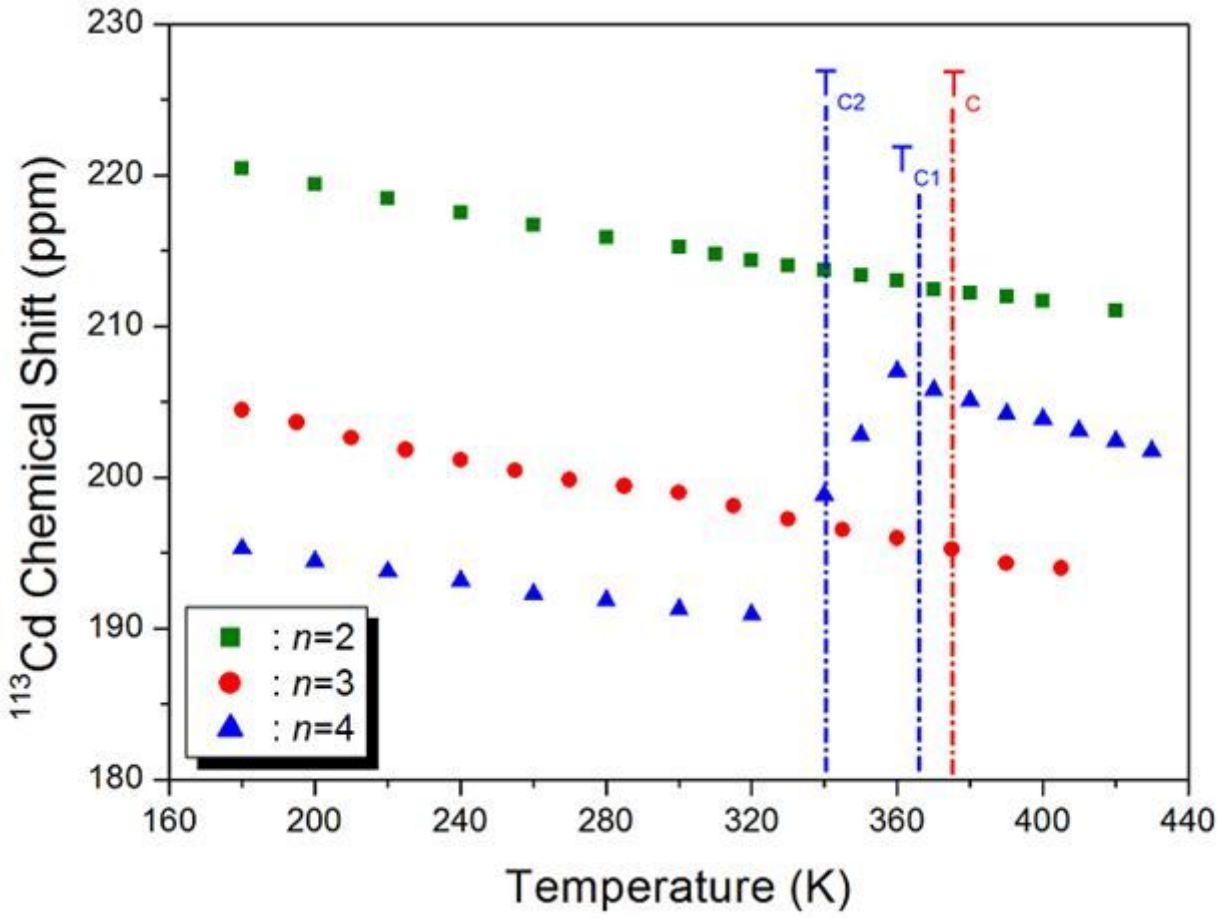

Figure 12

113Cd MAS NMR chemical shifts of [NH3(CH2)nNH3]CdCl4 (n=2, 3, and 4) as a function of temperature.

Supplementary Files

This is a list of supplementary files associated with this preprint. Click to download.

- SupplementaryInformation.docx